UNIVERSITY OF CRETE

BACHELOR'S THESIS

Dynamics of qubit chains coupled to non-Markovian reservoirs

Author:
Ioannis Stergou

Supervisor:
Prof. Peter Labropoulos

A thesis submitted in fulfillment of the requirements for the degree of Bachelor of Science

in the

Department of Physics

June 19, 2024

UNIVERSITY OF CRETE

Abstract

Department of Physics

Bachelor of Science

Dynamics of qubit chains coupled to non-Markovian reservoirs

by Ioannis Stergou

We offer a comprehensive assessment of non-Markovianity (DNM) within an XX chain of interacting qubits linked to a reservoir. Our investigation incorporates diverse quantum state distance (QSD) measures and considers various non-Markovian spectral densities, including the Lorentzian squared. This approach aims to provide a robust evaluation of DNM. By constructing the density matrix of the open chain without relying on a master equation, we analyze the dynamics of QSD measures between Markovian and non-Markovian damping scenarios. Recognizing that conventional QSD measures often presume trace-preserving density matrices, we adapt them to accommodate damped traces in open systems. Our findings not only demonstrate consistent outcomes across different QSD measures but also reveal intricate interactions between qubit-qubit coupling, non-Markovian damping, and entanglement dynamics, particularly notable when exploring the implications of the Lorentzian squared spectral density.

Acknowledgements

I would like to express my deepest gratitude to my supervisor, Prof. Peter Lambropoulos, for his invaluable guidance, support, and understanding throughout my research. His teachings in physics have been instrumental to my progress. I am also profoundly thankful to George Mouloudakis for his assistance with coding and his unwavering eagerness to help with any issues I encountered.

Contents

List of Figures

Dedicated to my family…

Chapter 1

Introduction

Spin chains represent models of physical systems of relevance to a broad class of phenomena ranging from statistical mechanics to quantum information and computing (Paganelli et al., 2013). Important aspects related to quantum information pertain to perfect or faithful state transfer from one end to the other of a chain. Physical realizations of such chains can vary, depending on the particular application. Examples, among others, are quantum dots, Josephson junctions, etc. Irrespective of the particular application, the ends of the chain, if not the entire chain, will be connected to an external environment which entails dissipation. In addition to loss, inherent in dissipation, decoherence and loss of entanglement are issues of fundamental importance to quantum information. In that connection, the dynamics of spin chains connected to external environments (reservoirs) represents a versatile tool for the study of the effect of environment on the quantum system.

The above mentioned dynamics depends very strongly on a very impactful property of the reservoir, namely its Markovianity or lack of it. Broadly speaking, a reservoir is Markovian if the memory of any excitation transferred from the system to the reservoir is lost instantly. In general terms, this is the case of a reservoir, with smooth and slowly varying density of states, coupled to the system weakly. A departure from the above two conditions makes the reservoir non-Markovian, which entails the possibility of excitation exchange between system and reservoir, at least for some finite time. Since more often than not, in real physical implementations of quantum systems involves connections to non-Markovian reservoirs, the resulting effect has been of central importance in current studies. A basic question in such studies is: How much is the dynamics affected by the departure of the reservoir from Markovian.

A recent paper (Mouloudakis, Ilias, and Lambropoulos, 2022), presented the dynamics of an XX chain, driven by non-Markovian reservoirs at both ends. They have reported results on the dynamics of the chain driven by reservoirs of Lorentzian as well as Ohmic spectral densities, in the single excitation case. Examining the time evolution of the initially excited spin (qubit), they pointed out that under Ohmic driving, the time evolution of the population seemed to resemble the Markovian more than that for Lorentzian. Since there are several measures of Markovianity in the literature, that system offers the possibility of a quantitative assessment of the Markovianity of different reservoirs.

The purpose of this thesis, is to evaluate the "degree of Markovianity" of different reservoirs coupled to an XX chain of various lengths. When studying non-Markovian reservoirs, it is most common in the literature to use Lorentzian (Weiss, 2001, Mouloudakis and Lambropoulos, 2021) and Ohmic (Leggett et al., 1987, Leggett et al., 1995, Zou et al., 2020) spectral densities. To that, we add the square of the Lorentzian spectral density, an unsual reservoir that has not been examined in this context but has some really surprising qualities. Our first task, is to calculate the

time evolution of the system under each reservoir, one of which is Markovian. After that, we work out the difference of the state of the system evolved under a given non-Markovian reservoir from the state evolved under the Markovian one. That difference and its time evolution is what we refer to as "Degree of Markovianity" (DM) of the given reservoir. The time evolution of the system has been calculated using Schrödinger's equations of motion within the single excitation subspace. The solutions have been obtained numerically using Python and Mathematica scripts.With the numerical solutions of the transformed amplitudes in hand, we calculate the density matrix elements of the system, the diagonal matrix elements of which are the probabilities of finding the chain in one of its states.

Our objective, as stated in the title, is to quantify the Markovianity of a given reservoir. To that end, we need a tool that measures the difference or "distance" between states. A variety of measures appropriate as tools for our task have been proposed over the years (Rivas, Huelga, and Plenio, 2014, Dajka, Łuczka, and Hänggi, 2011). In our calculations, we use three different Quantum State Distance (QSD) measures, namely the Trace Distance (TD), Hellinger Distance (HD) and Bures Distance (BD). In view of such diversity of expressions for the QSD, we have added an additional aspect to our project, which is a comparative analysis of the three stated QSD measures. To the best of our knowledge, this seems to be the most extensive comparative study of those measures, in the context of a realistic quantum system.

A large part of our results have already appeared in Mouloudakis, Stergou, and Lambropoulos, 2023, with the exception of the time evolution of entanglement which represents the content of chapter 3, section 3.3 of this thesis.

The outline of this thesis is as follows. In Chap. 2 we provide the theoretical description of our problem in terms of the time-dependent Schrödinger's equation. We also give a brief summary of the QSD measures that have been employed. In Chap. 3 we present results for a system of one qubit and a 5-qubit chain. We do in addition analyse the time evolution of qubit-qubit entanglement in a 6-qubit chain. In Chap. 4 we study in further detail the unusual properties of the Lorentzian squared reservoir. Finally, in Chap. 5 we provide some concluding remarks as well as future directions related to our work.

Chapter 2

Theory

2.1 The model

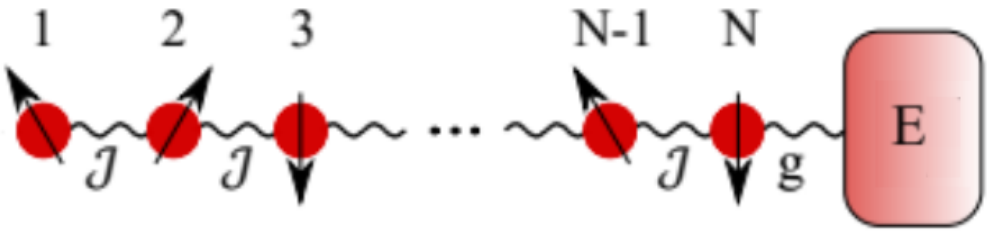

FIGURE 2.1: Schematic presentation of the system at study. A Heisenberg XX spin chain of arbitrary length is coupled to a reservoir at its edge.

Our system consists of an N qubit chain interacting with an environment E through its last qubit, with coupling strength g. The interaction between each pair of neighboring qubits in the chain is denoted by J.Time is measured in units of 1/J. A schematic presentation of our system is depicted in Fig. 2.1. The Hamiltonian of the system is given by ($\hbar = 1$):

$$H = H_S + H_E + H_I \tag{2.1}$$

where $H_S = H_{S_0} + H_S^{'}$ is the Hamiltonian of the spin chain:

$$H_{S_0} = \omega_e \sum_{i=1}^{N} |e\rangle_{ii} \langle e| + \omega_g \sum_{i=1}^{N} |g\rangle_{ii} \langle g|$$
$$H_S^{'} = \sum_{i=1}^{N-1} \frac{J}{2} (\sigma_i^+ \sigma_{i+1}^- + \sigma_i^- \sigma_{i+1}^+)$$

H_E is the Hamiltonian of the environment:

$$H_E = \sum_{\lambda} \omega_\lambda \alpha_\lambda^\dagger \alpha_\lambda \tag{2.2}$$

and H_I is the interaction of the spin chain with the reservoir:

$$H_I = \sum_{\lambda} g_\lambda (\alpha_\lambda \sigma_N^+ + \alpha_\lambda^\dagger \sigma_N^-) \tag{2.3}$$

where ω_g and ω_e are, respectively, the energies of the ground and excited state of each spin, ω_λ is the energy of the λ-mode photon of the environment, $\alpha_\lambda and\ \alpha_\lambda^\dagger$ are the annihilation and creation operators of the environment, and $\sigma_i^+ = |e\rangle_{ii}\langle g|$ and $\sigma_i^- = |g\rangle_{ii}\langle e|$, $i = 1, ..., N$ are the qubit raising and lowering operators, respectively.

As stated in the introduction, we will be studying the system in the single-excitation space. The total wavefunction of the system is:

$$|\Psi(t)\rangle = \sum_{i=1}^{N} c_i(t)\,|\psi_i\rangle + \sum_\lambda c_\lambda^E(t)\left|\psi_\lambda^E\right\rangle \tag{2.4}$$

where,

$$|\psi_i\rangle = |g\rangle_1 |g\rangle_2 \cdots |g\rangle_{i-1} |e\rangle_i |g\rangle_{i+1} \cdots |g\rangle_N |0\rangle_E$$
$$\left|\psi_\lambda^E\right\rangle = |g\rangle_1 |g\rangle_2 \ldots |g\rangle_N |00...01_\lambda 0...00\rangle_E$$

are, respectively, the state in which the i^{th} site is excited and the state in which the environment has an excitation in the λ mode.

For convenience purposes, we will be working in the interaction picture.To do that, we rewrite the Hamiltonian of the system as $H = H_0 + H^{'}$, with $H_0 = H_{S_0} + H_E$ and $H^{'} = H_S^{'} + H_I$, and apply the transformation $U(t) = e^{iH_0 t}$ to the states of the system. The transformed amplitudes in the interaction picture are $\tilde{c_i}(t) = c_i(t)e^{i[\omega_e + (N-1)\omega_g]t}$ for the qubits and $\tilde{c_\lambda^E}(t) = c_\lambda^E(t)e^{i[N\omega_g + \omega_\lambda]t}$ for the environment. Using Schrödinger's equation in the interaction picture:

$$i\frac{\partial}{\partial t}\left|\tilde{\Psi}(t)\right\rangle = H^{'}\left|\tilde{\Psi}(t)\right\rangle \tag{2.5}$$

we get the equations of motion for the transformed amplitudes:

$$i\frac{\partial \tilde{c_i}}{\partial t} = \sum_{m=1}^{N} \tilde{c_m}(t)\,\langle\psi_i|\,H_S^{'} + H_I\,|\psi_m\rangle + \sum_\lambda e^{i(\omega_e - \omega_g - \omega_\lambda)t}\tilde{c_\lambda^E}(t)\,\langle\psi_i|\,H_S^{'} + H_I\left|\psi_\lambda^E\right\rangle \tag{2.6}$$

$$i\frac{\partial \tilde{c_\lambda^E}}{\partial t} = \sum_{m=1}^{N} e^{i(\omega_\lambda + \omega_g - \omega_e)t}\tilde{c_m}(t)\left\langle\psi_\lambda^E\right|H_S^{'} + H_I\,|\psi_m\rangle + \sum_{\lambda^{'}} \tilde{c_{\lambda^{'}}^E}(t)\left\langle\psi_\lambda^E\right|H_S^{'} + H_I\left|\psi_{\lambda^{'}}^E\right\rangle \tag{2.7}$$

which, after some tedious algebra, reduce to :

$$i\frac{\partial \tilde{c_i}}{\partial t} = \sum_{m=1}^{N} \tilde{c_m}(t)\,\langle\psi_i|\,H_S^{'}\,|\psi_m\rangle \qquad i \neq N \tag{2.8}$$

$$i\frac{\partial \tilde{c_N}}{\partial t} = \sum_{m=1}^{N} \tilde{c_m}(t)\,\langle\psi_N|\,H_S^{'}\,|\psi_m\rangle + \sum_\lambda g(\omega_\lambda)e^{-i\Delta_\lambda t}\tilde{c_\lambda^E}(t) \tag{2.9}$$

$$i\frac{\partial \tilde{c_\lambda^E}}{\partial t} = e^{i\Delta_\lambda t}\tilde{c_N}(t)g(\omega_\lambda) \tag{2.10}$$

where $\Delta_\lambda \equiv \omega_\lambda - (\omega_e - \omega_g) \equiv \omega_\lambda - \omega_{eg}$. Integrating equation (2.10), under the assumption that $\tilde{c_\lambda^E}(0) = 0$, and substituting back to equation (2.9), yields:

$$\frac{\partial \tilde{c_N}(t)}{\partial t} = -i \sum_{m=1}^{N} \tilde{c_m}(t) \langle \psi_N | H_S^{'} | \psi_m \rangle - \int_0^t \sum_{\lambda} e^{-i\Delta_\lambda (t-t^{'})} [g(\omega_\lambda)]^2 \tilde{c_N}(t^{'}) \, dt' \tag{2.11}$$

In the limit of a continuous distribution, the summations convert into integrals according to $\sum_\lambda [g(\omega_\lambda)]^2 \rightarrow \int J(\omega_\lambda) \, d\omega_\lambda$, where $J(\omega_\lambda)$ is the spectral density of the environment. So far, we have not specified the environment in use and thus, the resulting set of differential equations are correct for any possible spectral density:

$$\frac{\partial \tilde{c_i}}{\partial t} = -i \sum_{m=1}^{N} \tilde{c_m}(t) \langle \psi_i | H_S^{'} | \psi_m \rangle \qquad i \neq N \tag{2.12}$$

$$\frac{\partial \tilde{c_N}(t)}{\partial t} = -i \sum_{m=1}^{N} \tilde{c_m}(t) \langle \psi_N | H_S^{'} | \psi_m \rangle - \int_0^t R(t-t^{'}) \tilde{c_N}(t^{'}) \, dt' \tag{2.13}$$

where we define

$$R(t) \equiv \int_0^\infty J(\omega_\lambda) e^{-i\Delta_\lambda t} \, d\omega_\lambda \tag{2.14}$$

In the subsections that follow, we present the spectral densities of the reservoirs that use for our calculations.

2.1.1 Markovian Reservoir

A simple way to emulate a markovian reservoir, is to replace the integral part of equation (2.13) with an exponential decay. Making that change, the differential equations for the Markovian case take the form:

$$\frac{\partial \tilde{c_i}}{\partial t} = -i \sum_{m=1}^{N} \tilde{c_m}(t) \langle \psi_i | H_S^{'} | \psi_m \rangle \qquad i \neq N \tag{2.15}$$

$$\frac{\partial \tilde{c_N}(t)}{\partial t} = -i \sum_{m=1}^{N} \tilde{c_m}(t) \langle \psi_N | H_S^{'} | \psi_m \rangle - \frac{\Gamma}{2} \tilde{c_N}(t) \tag{2.16}$$

The reason for $\frac{\Gamma}{2}$ and not Γ, is that we want the populations to decay with rate Γ and for that to happen the amplitudes have to decay with $\frac{\Gamma}{2}$.

2.1.2 Lorentzian Reservoir

Our first Non-Markovian environment has a Lorentzian spectral density given by:

$$J(\omega_\lambda) = \frac{g^2}{\pi} \frac{\frac{\Gamma}{2}}{(\omega_\lambda - \omega_c)^2 + (\frac{\Gamma}{2})^2} \tag{2.17}$$

where g is the coupling strength between the last qubit and the reservoir in units of frequency and Γ, ω_c are, respectively, the width and the peak frequency of the distribution.

For analytical simplification of equation (2.14), we extend the lower limit of the integration over frequency from 0 to -∞. For that to be justified, the distribution must have negligible extension to negative frequencies. The necessary condition for

this is $\Gamma << \omega_c$. If that condition is met, the frequency integral can be calculated analytically, yielding:

$$R(t) = \frac{g^2}{\pi}\frac{\Gamma}{2}\int_{-\infty}^{+\infty}\frac{e^{-i(\omega_\lambda-\omega_{eg})t}}{(\omega_\lambda-\omega_c)^2+(\frac{\Gamma}{2})^2}\,d\omega_\lambda = g^2 e^{-i\Delta_c t}e^{-\frac{\Gamma}{2}t} \tag{2.18}$$

where $\Delta_c \equiv \omega_c - \omega_{eg}$. In our calculations, we always assume that $\Delta_c = 0$ to make things simpler.

Integro-differential equations are usually very hard for computers to solve numerically. Depending on the initial conditions, it could take days for a typical computer to solve a set of differential equations with integrals in it. It is therefore necessary to eliminate the integrals whenever it is possible. Thankfully, we can eliminate the integral in this situation by introducing a new variable $x = \int_0^t R(t-t')\tilde{c_N}(t')\,dt'$. Substituting $R(t-t')$ with its value for the Lorentzian spectral density, while keeping in mind that we have assumed $\Delta_c = 0$, yields:

$$x = e^{-\frac{\Gamma}{2}t}\int_0^t g^2 e^{\frac{\Gamma}{2}t'}\tilde{c_N}(t')\,dt' \tag{2.19}$$

Now if we call the integral in equation (2.19) I and differentiate both parts we get:

$$\frac{\partial x}{\partial t} = -\frac{\Gamma}{2}e^{-\frac{-\Gamma}{2}t}I + g^2\tilde{c_N}(t) \tag{2.20}$$

and solving (2.19) for I gives:

$$I = e^{-\frac{\Gamma}{2}t}x \tag{2.21}$$

By substituting I in equation (2.20) we get a new differential equation for x that is coupled with the ones for the amplitudes. We can think of x as an assistant variable, it's solution does not interest us but it helps us solve for the amplitudes. The set of differential equations for the Lorentzian case is:

$$\frac{\partial\tilde{c_i}}{\partial t} = -i\sum_{m=1}^{N}\tilde{c_m}(t)\,\langle\psi_i|\,H_S'\,|\psi_m\rangle \qquad i \neq N \tag{2.22}$$

$$\frac{\partial\tilde{c_N}(t)}{\partial t} = -i\sum_{m=1}^{N}\tilde{c_m}(t)\,\langle\psi_N|\,H_S'\,|\psi_m\rangle - x \tag{2.23}$$

$$\frac{\partial x}{\partial t} = -\frac{\Gamma}{2}x + g^2\tilde{c_N}(t) \tag{2.24}$$

2.1.3 Lorentzian squared

Our second pick for a Non-Markovian environment, is the square of the Lorentzian. Though not widely known, Lorentzian squared spectral densities could have applications in Mössbauer spectroscopy (Whipple, 1981). The spectral density is given by:

$$J(\omega_\lambda) = \frac{2g^2}{\pi}\frac{(\frac{\Gamma}{2})^3}{[(\omega_\lambda-\omega_c)^2+(\frac{\Gamma}{2})^2]^2} \tag{2.25}$$

where g is the coupling strength between the last qubit and the reservoir in units of frequency and Γ, ω_c are, respectively, the width and the peak frequency of the distribution. Now, following the same procedure as the Lorentzian, we can calculate R(t):

$$R(t) = \frac{2g^2}{\pi}\frac{\Gamma^3}{8}\int_{-\infty}^{+\infty}\frac{e^{-i(\omega_\lambda-\omega_{eg})t}}{[(\omega_\lambda-\omega_c)^2+(\frac{\Gamma}{2})^2]^2}\,d\omega_\lambda = g^2e^{-i\Delta_c t}(\frac{\Gamma}{2}t+1)e^{-\frac{\Gamma}{2}t} \tag{2.26}$$

then assume $\Delta_c = 0$, substitute into x, call the integral I_1 and differentiate both sides like we did in the previous subsection:

$$x = g^2\int_0^t\left(\frac{\Gamma}{2}t-\frac{\Gamma}{2}t'+1\right)e^{-\frac{\Gamma}{2}(t-t')}\tilde{c_N}(t')\,dt' \tag{2.27}$$

$$I_1 = \frac{x}{g^2} \tag{2.28}$$

$$\frac{\partial x}{\partial t} = g^2\left[\tilde{c_N}(t)+\frac{\Gamma}{2}\int_0^t e^{-\frac{\Gamma}{2}(t-t')}\tilde{c_N}(t')\,dt'-\frac{\Gamma}{2}I_1\right] \tag{2.29}$$

Because of the integral in equation (2.29) we must repeat the procedure. Introducing a new variable,

$$y = \int_0^t e^{-\frac{\Gamma}{2}(t-t')}\tilde{c_N}(t')\,dt' \tag{2.30}$$

equation (2.29) becomes:

$$\frac{\partial x}{\partial t} = g^2\left(\tilde{c_N}(t)+\frac{\Gamma}{2}y-\frac{\Gamma}{2}I_1\right) \tag{2.31}$$

Substituting (2.28) into (2.31) we get,

$$\frac{\partial x}{\partial t} = g^2\left(\tilde{c_N}(t)+\frac{\Gamma}{2}y-\frac{x}{g^2}\right) \tag{2.32}$$

It is obvious that a differential equation for y is demanded for the system to have a solution. We can get that by calling the integral part of y I_2 and differentiating both parts as we did with x:

$$y = e^{-\frac{\Gamma}{2}t}\int_0^t e^{\frac{\Gamma}{2}t'}\tilde{c_N}(t')\,dt' \tag{2.33}$$

$$I_2 = e^{\frac{\Gamma}{2}t}y \tag{2.34}$$

$$\frac{\partial y}{\partial t} = -\frac{\Gamma}{2}e^{-\frac{\Gamma}{2}t}I_2+\tilde{c_N}(t) \tag{2.35}$$

Finally, we substitute (2.34) into (2.35) and after some rearrangements of the terms we get the final set of coupled differential equations for the squared Lorentzian spectral density:

$$\frac{\partial\tilde{c_i}}{\partial t} = -i\sum_{m=1}^{N}\tilde{c_m}(t)\left\langle\psi_i\right|H_S'\left|\psi_m\right\rangle \qquad i\neq N \tag{2.36}$$

$$\frac{\partial\tilde{c_N}(t)}{\partial t} = -i\sum_{m=1}^{N}\tilde{c_m}(t)\left\langle\psi_N\right|H_S'\left|\psi_m\right\rangle - x \tag{2.37}$$

$$\frac{\partial x}{\partial t} = -\frac{\Gamma}{2}x+\frac{\Gamma}{2}g^2y+g^2\tilde{c_N}(t) \tag{2.38}$$

$$\frac{\partial y}{\partial t} = -\frac{\Gamma}{2}y+\tilde{c_N}(t) \tag{2.39}$$

2.1.4 Ohmic Reservoir

Our last pick for a Non-Markovian reservoir, is described by an Ohmic spectral density according to the relation:

$$J(\omega_\lambda) = \mathcal{N} g^2 \omega_c \left(\frac{\omega_\lambda}{\omega_c}\right)^{\mathcal{S}} e^{-\frac{\omega_\lambda}{\omega_c}} \tag{2.40}$$

where g is the qubit-environment coupling constant in units of frequency, ω_c is the Ohmic cut-off frequency and S is the Ohmic parameter. Depending on the value of the Ohmic parameter, the spectrum of the reservoir is sub-Ohmic $\mathcal{S} < 1$, Ohmic $\mathcal{S} = 1$ or super-Ohmic $\mathcal{S} > 1$. $\mathcal{N}$ is a normalization constant given by the relation $\mathcal{N} = \frac{1}{(\omega_c)^2 \Gamma(1+\mathcal{S})}$, where $\Gamma(z)$ is the gamma function. Using equation (2.40) in (2.14), we can get an analytical expression for R(t):

$$R(t) = \mathcal{N} g^2 \omega_c \int_0^\infty \left(\frac{\omega_\lambda}{\omega_c}\right)^{\mathcal{S}} e^{-\frac{\omega_\lambda}{\omega_c}} e^{-i(\omega_\lambda - \omega_{eg})t}\, d\omega_\lambda = g^2 e^{i\omega_{eg}t} \left(i\omega_c t + 1\right)^{-1-\mathcal{S}} \tag{2.41}$$

Sadly, the method used in the previous subsections to eliminate the integrals does not apply here and therefore the set of differential equations for solution is the following:

$$\frac{\partial \tilde{c_i}}{\partial t} = -i \sum_{m=1}^{N} \tilde{c_m}(t) \left\langle \psi_i \right| H_S^{'} \left| \psi_m \right\rangle \qquad i \neq N \tag{2.42}$$

$$\frac{\partial \tilde{c_N}(t)}{\partial t} = -i \sum_{m=1}^{N} \tilde{c_m}(t) \left\langle \psi_N \right| H_S^{'} \left| \psi_m \right\rangle - \int_0^t g^2 e^{i\omega_{eg}(t-t^{'})} \left(i\omega_c (t-t^{'}) + 1\right)^{-1-\mathcal{S}} \tilde{c_N}(t^{'})\, dt' \tag{2.43}$$

2.2 QSD Measures

Markovian processes tend to continuously reduce the distinguishability between any two states, while the essential property of non-Markovian behavior is the growth of this distinguishability. Knowing that, one can quantify the degree of non-Markovian behaviour using quantum distance measures.

In quantum mechanics, a distance measure evaluates the extent to which two quantum states are "close" to each other. In a broad sense, two states are close to each other if their distance is small. Unfortunately, there is no single, ideal measure of distinguishability of different states. There are no criteria that make a distance measure better than another one.

One widely known distance measure, is the fidelity. It is notably used in quantum information theory and it expresses the probability that one state will pass a test to identify as the other. Given two density operators ρ and σ, the fidelity is generally defined by one of the three expressions that we list below (Jozsa, 1994,Uhlmann, 2000,Mendonça et al., 2008):

$$F_1(\rho, \sigma) = \left(\mathrm{Tr}\sqrt{\sqrt{\rho}\sigma\sqrt{\rho}}\right)^2 \tag{2.44}$$

$$F_2(\rho, \sigma) = \mathrm{Tr}\sqrt{\sqrt{\rho}\sigma\sqrt{\rho}} = \sqrt{F_1(\rho, \sigma)} \tag{2.45}$$

$$F_3(\rho,\sigma) = \mathrm{Tr}(\rho,\sigma) \tag{2.46}$$

where, for a positive semidefinite matrix M, $\sqrt{M}$ denotes its unique positive square root. While there are subtle differences in the descriptions of the square root of a matrix across various sources, we opt for the definition that is widely prevalent in the literature on quantum information which is the positive one (Nielsen and Chuang, 2000).

Before delving into the discussion of QSD measures, it is essential to provide a significant clarification regarding our approach and treatment. As we demonstrated in the previous section, the amplitudes of the wave-function of the system are obtained from the time-dependent Schrödinger equation after having eliminated the degrees of freedom of the reservoir. Using the time-dependent amplitudes, we construct the reduced operator of the system which is needed in all expressions of QSD. This approach offers the advantage of being applicable to any reservoir type, bypassing the need for a master equation, which is generally unavailable, particularly for non-Markovian reservoirs. However, there is a trade-off for this advantage. During the elimination of the reservoir continuum, the populations of ground states are discarded resulting in the density operator describing only the excitation. This situation has implications for the system density operator. The scenario is analogous to the treatment of the decay of a discrete state coupled to a continuum (Lambropoulos and Petrosyan, 2007, Goldberger and Watson, 1964). However, in this context we are dealing with the excitation of a chain. Therefore, the reduced density operator essentially depicts the time evolution of the excitation, which, as expected, gradually dissipates into the reservoir in the long-term.

Expressions for F or QSD are often assumed, either impicitly or explicitly to involve density operators with trace equal to unity. However, given that our approach results in the decay of the trace of the reduced density operator, the expression for QSD needs to be appropriately adjusted. The concept of distance between two quantum states can be introduced in a variety of ways. Below we present the three quantum distance measures that we use for this project :

(1) Our first pick, the Trace distance, defined by:

$$D_T(\rho,\sigma) = \frac{1}{2}Tr\|\rho-\sigma\| = \frac{1}{2}Tr\sqrt{(\rho-\sigma)^\dagger(\rho-\sigma)} \tag{2.47}$$

where for a positive semidefinite matrix A, $\sqrt{A}$ denotes a positive semidefinite matrix B such that $B^2 = A$. Note that B is a unique matrix so defined. The trace distance D_T represents a natural metric on the space of density matrices, satisfying $0 \leq D_T \leq 1$.

To get a grasp of its physical interpretation, suppose that Alice prepares a quantum system in one of two states ρ_1 and ρ_2, each with probability $\frac{1}{2}$, and gives the system to Bob who performs a measurement to decide whether the system was in the state ρ_1 or ρ_2. One can show that the quantity $\frac{1}{2}[1 + D_T(\rho_1,\rho_2)]$ is then equal to the probability that Bob can successfully identify the state of the system. Thus, the trace distance can be interpreted as a measure for the distinguishability of two quantum states.

The trace distance is likely the most important measure for distinguishing Markovian from non-Markovian behaviour. Just by looking at the rate of change of the trace distance,

$$\sigma(t,\rho_{1.2}(0)) = \frac{\partial}{\partial t}D_T(\rho_1(t),\rho_2(t)) \tag{2.48}$$

we can tell if a quantum process is Markovian or not as it has been shown that for all Markovian processes $\sigma \leq 0$ holds true. If there is a physical process, for which a pair of initial states $\rho_{1,2}(0)$ and a certain time t such that $\sigma(t, \rho_{1,2}(0)) > 0$ exists, it is said to be non-Markovian. Physically speaking, this indicates that the distinguishability of the pair of states increases at certain times for non-Markovian dynamics, which can be interpeted as a back-flow of information from the environment to the system.

(2) Our second choice, the Bures distance is a metric defined using the fidelity. The Bures QSD is usually defined as $D_B^2(\rho, \sigma) \equiv 2\left[1 - \sqrt{F_1(\rho, \sigma)}\right]$, which in view of Eqn. (2.45) can be written as

$$D_B^2(\rho, \sigma) = 2\left[1 - F_2(\rho, \sigma)\right] \tag{2.49}$$

from which we obtain

$$D_B(\rho, \sigma) = \sqrt{2}\left[1 - \mathrm{Tr}\sqrt{\sqrt{\rho}\sigma\sqrt{\rho}}\right]^{1/2} \tag{2.50}$$

As long as $\mathrm{Tr}\,\rho = \mathrm{Tr}\,\sigma = 1$ is satisfied for all times, this expression is valid because if in any distance measure we set $\rho = \sigma$, we should obtain zero. In our case though as stated before, we have a dissipation of the excitation over time which corresponds to the traces decaying to zero which, for the case $\rho = \sigma$, yields the nonphysical value $\sqrt{2}$. In order to move past that contradiction, we will use the following modified version of the Bures QSD:

$$D_B(\rho, \sigma) = \sqrt{2}\left[\frac{1}{2}(\mathrm{Tr}\,\rho + \mathrm{Tr}\,\sigma) - \mathrm{Tr}\sqrt{\sqrt{\rho}\sigma\sqrt{\rho}}\right]^{1/2} \tag{2.51}$$

This is the expression we are using for the Bures QSD for our project. In the long time limit and in the presence of dissipation, the modified Bures distance tends to zero as it should.

(3) Lastly, among the plethora of distances between states there are measures whose definition come from the statistical interpretation of quantum states. The so-called Hellinger distance is one of them. It is defined as :

$$D_H^2(\rho, \sigma) = Tr(\sqrt{\rho} - \sqrt{\sigma})^2 \tag{2.52}$$

which upon expansion of the square reduces to

$$D_H^2(\rho, \sigma) = \mathrm{Tr}\,\rho + \mathrm{Tr}\,\sigma - 2\,\mathrm{Tr}\big(\sqrt{\rho}\sqrt{\sigma}\big) \tag{2.53}$$

Just like the Bures QSD, if the density operators are unity, Eqn.(2.53) reduces to $D_H^2 = \sqrt{2}\left[1 - \mathrm{Tr}\big(\sqrt{\rho}\sqrt{\sigma}\big)\right]$, which then leads to the expression

$$D_H = \sqrt{2}\left[1 - \mathrm{Tr}\big(\sqrt{\rho}\sqrt{\sigma}\big)\right]^{1/2} \tag{2.54}$$

This is the expression for the Hellinger distance measure that is typically used in the bibliography. However, in order to account for the dissipation of the populations we have :

$$D_H = \left[\mathrm{Tr}\,\rho + \mathrm{Tr}\,\sigma - 2\,\mathrm{Tr}\big(\sqrt{\rho}\sqrt{\sigma}\big)\right]^{1/2} \tag{2.55}$$

We can see that Eqn.(2.54) leads to the value $\sqrt{2}$ as $t \to \infty$. This is not physically possible as it does not account for the decay of the traces of the density operators. On the other hand, Eqn.(2.55) correctly yields zero for the distance between the two

states in the limit of $t \to \infty$. That is why for our purpose we use Eqn.(2.55) for the Hellinger QSD.

Chapter 3

Results

In this chapter, we present results for two different systems,a 1-qubit and a 5-qubit chain. We divide this chapter into three sections.

In section 3.1, we show the time dynamics of the populations with each reservoir at the edge of the chain. To get these results, we have written a python script (for each reservoir) that constructs the differential equations of the amplitudes and solves them numerically using the RK45 method. After that, it is easy to construct the density matrix elements using the amplitude solutions. Due to computational difficulties when using integro-differential equations, any results regarding the Ohmic spectral densities are calculated by Mouloudakis utilizing the Laplace transform just like in one of his recent papers (Mouloudakis, Ilias, and Lambropoulos, 2022).

In section 3.2, we use all three QSD measures to calculate the distance of the Markovian solution from each non-Markovian solution over time. The thought behind this is simple, given two non-Markovian reservoirs we can tell which one is "more non-Markovian" by comparing their distances with the Markovian one.

Knowing that our end goal is to compare each reservoir with the Markovian one, we need to make that comparison as "fair" as possible. It is evident, that making direct comparison between different scenarios, such as the evolution under a Markovian reservoir with damping rate Γ and a Lorentzian reservoir with parameters g, Γ_L, Δ_c, would be futile. To ensure a meaningful comparison, we propose adopting a common feature shared by all reservoirs involded in the comparison. Specifically, given that for all reservoirs the excitation of all qubits will ultimately decay to zero and without claim to uniqueness, we set the parameters of the various reservoirs to achieve approximately the same half-life for the excitation of the first qubit as it would have under a Markovian reservoir with a specified Γ_M.

This choice allows some flexibility in selecting the parameter g, which expresses the coupling strength between the last qubit of the chain and the non-Markovian reservoir. In both single and 5-qubit scenarios, and for all considered non-Markovian reservoirs, we set the parameter g to the value $g = 1$. Notably, the parameters determining the lifetime of the excitation in the chain are chosen to ensure that the period of population oscillations between the last qubit and the reservoir is shorter than this lifetime.

Finally, in section 3.3 we study the qubit-qubit entanglement behaviour in a 6-qubit chain.

3.1 Populations

3.1.1 1-qubit theoritical backround

We start by looking at the simplest system first, which consists of one qubit coupled to a reservoir. The reason for that is that the differential equation of motion for a single qubit can be written with ease, and it is even possible to obtain analytical expressions for the amplitudes and populations in some of the reservoirs.

(a) Starting with the Markovian case, using equation (2.16) for N=1 we get:

$$\frac{\partial \tilde{c_1}}{\partial t} = -\frac{\Gamma}{2}\tilde{c_1}(t) \tag{3.1}$$

which upon solution, with initial condition $\tilde{c_1}(0) = 1$, yields:

$$\tilde{c_1}(t) = e^{-\frac{\Gamma}{2}t} \tag{3.2}$$

$$|\tilde{c_1}(t)|^2 = e^{-\Gamma t} \tag{3.3}$$

As we see, a system of one qubit connected to a Markovian reservoir has an exact solution which is a simple exponential decay with the population of the qubit decaying to the environment with rate Γ.

(b) Moving on to the Lorentzian case, equations (2.23), (2.24) for N=1 become :

$$\frac{\partial \tilde{c_1}}{\partial t} = -x \tag{3.4}$$

$$\frac{\partial x}{\partial t} = -\frac{\Gamma}{2}x + g^2\tilde{c_1}(t) \tag{3.5}$$

which is a simple system of two coupled differential equations. Differentiating equation (3.4) and substituting into (3.5) we get the differential equation for the amplitude:

$$\frac{\partial^2 \tilde{c_1}}{\partial t^2} + \frac{\Gamma}{2}\frac{\partial \tilde{c_1}}{\partial t} + g^2\tilde{c_1} = 0 \tag{3.6}$$

Equation (3.6) is known as the problem of a damped harmonic oscillator and is solved using the exponential ansatz $\tilde{c_1}(t)\ e^{\lambda t}$ which results in :

$$\lambda^2 + \frac{\Gamma}{2}\lambda + g^2 = 0 \tag{3.7}$$

Depending on the value of the discriminant $\delta = \left(\frac{\Gamma}{2}\right)^2 - 4g^2$, we distinguish three cases:
i) Overdamped case for $\delta > 0$
ii) Critically damped case for $\delta = 0$
iii) Underdamped case for $\delta < 0$

In this project, we concentrate on g and Γ values that result in a negative discriminant. Moving further with the calculations and assuming that the discriminant is negative, it is simple to reach the following general solution:

$$\tilde{c_1}(t) = e^{-\frac{\Gamma}{4}t}\left(Ae^{i\frac{\delta}{2}t} + Be^{-i\frac{\delta}{2}t}\right) \tag{3.8}$$

We require two initial conditions in order to determine the values of A and B. The first one is the obvious $\tilde{c_1}(0) = 1$. The second one arrises from setting t=0 in the

definition of x which results in x(0)=0. Now setting t=0 in equation (3.4), provides us with a second initial condition which is $\frac{\partial \tilde{c_1}(0)}{\partial t} = 0$. After some trivial calculations we arrive at the results:

$$\tilde{c_1}(t) = e^{-\frac{\Gamma}{4}t}\left(\cos\frac{\delta}{2}t + \frac{\Gamma}{2\delta}\sin\frac{\delta}{2}t\right) \tag{3.9}$$

$$|\tilde{c_1}(t)|^2 = e^{-\frac{\Gamma}{2}t}\left[\left(\left(\frac{1}{2} - \frac{1}{8}\left(\frac{\Gamma}{\delta}\right)^2\right)\cos\delta t + \frac{\Gamma}{2\delta}\sin\delta t + \left(\frac{1}{2} + \frac{1}{8}\left(\frac{\Gamma}{\delta}\right)^2\right)\right)\right] \tag{3.10}$$

with $\delta = 4g^2 - \left(\frac{\Gamma}{2}\right)^2$.

(c) Following the same path, using equations (2.37), (2.38), (2.39) with N=1, we get a system of three coupled differential equations for the Lorentzian squared:

$$\frac{\partial \tilde{c_1}}{\partial t} = -x \tag{3.11}$$

$$\frac{\partial x}{\partial t} = -\frac{\Gamma}{2}x + \frac{\Gamma}{2}g^2 y + g^2\tilde{c_1}(t) \tag{3.12}$$

$$\frac{\partial y}{\partial t} = -\frac{\Gamma}{2}y + \tilde{c_1}(t) \tag{3.13}$$

Solving for $\tilde{c_1}$ we arrive at:

$$\frac{\partial^3 \tilde{c_1}}{\partial t^3} + \Gamma\frac{\partial^2 \tilde{c_1}}{\partial t^2} + \left[g^2 + \left(\frac{\Gamma}{2}\right)^2\right]\frac{\partial \tilde{c_1}}{\partial t} + \Gamma g^2\tilde{c_1}(t) = 0 \tag{3.14}$$

Unfortunately, there is no analytical solution for this differential equation. However, we can easily get numerical results if we specify the initial conditions which, applying the same reasoning as in the Lorentzian case, are as follows :

$$\tilde{c_1}(0) = 1$$
$$\frac{\partial \tilde{c_1}(0)}{\partial t} = 0$$
$$\frac{\partial^2 \tilde{c_1}(0)}{\partial t^2} = -g^2$$

(d) Finally, setting N=1 in equation (2.43) , gives rise to the equation of motion for the Ohmic case:

$$\frac{\partial \tilde{c_1}}{\partial t} = -\int_0^t g^2 e^{i\omega_{eg}(t-t')}\left(i\omega_c(t-t') + 1\right)^{-1-\mathcal{S}}\tilde{c_1}(t')\,dt' \tag{3.15}$$

As said in the previous chapter, the integral here can not be eliminated hence there is no analytical solution. Differential equations like these are known as integro-differential equations and can be solved numerically.

3.1.2 Numerical results and discussion

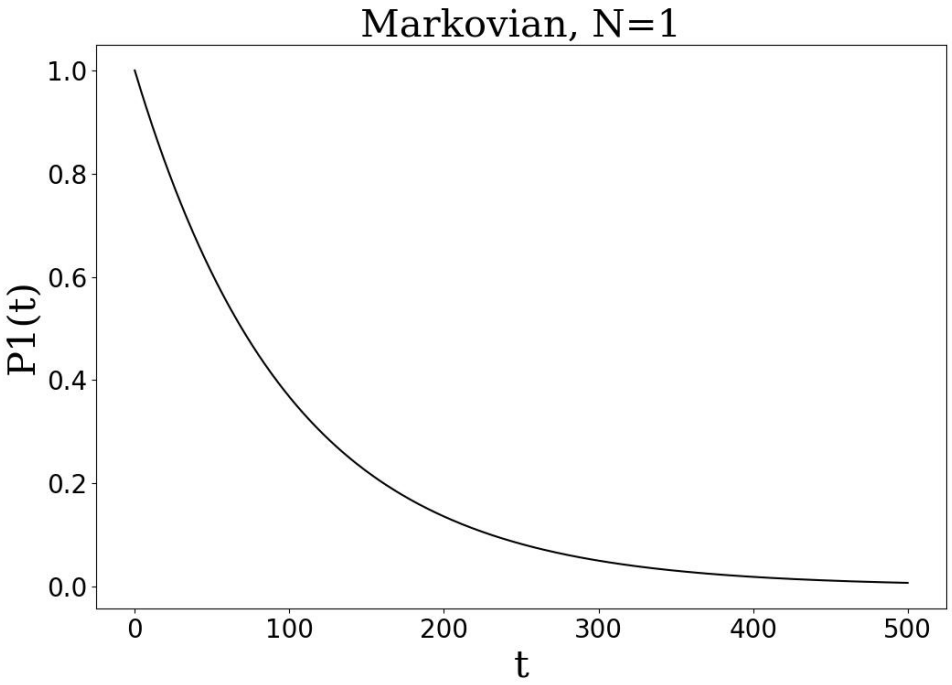

FIGURE 3.1: Dynamics of the populations of a qubit connected to a Markovian reservoir for $c_1(0) = 1$,$\Gamma = 0.01$, $J = 1$.

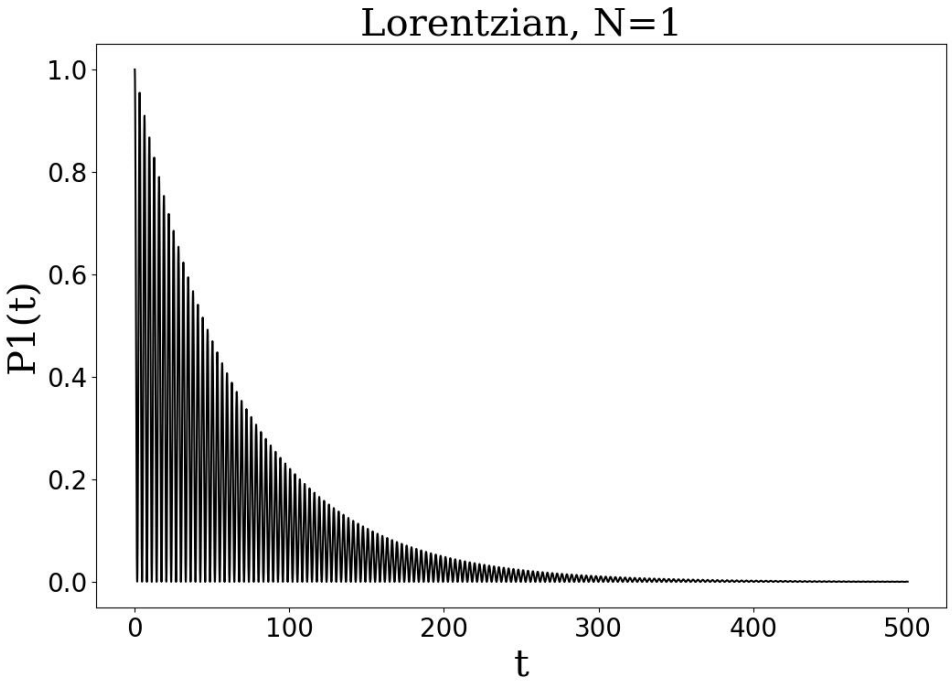

FIGURE 3.2: Dynamics of the populations of a qubit connected to a Lorentzian reservoir for $c_1(0) = 1$,$\Gamma = 0.03$, $g = 1$, $J = 1$.

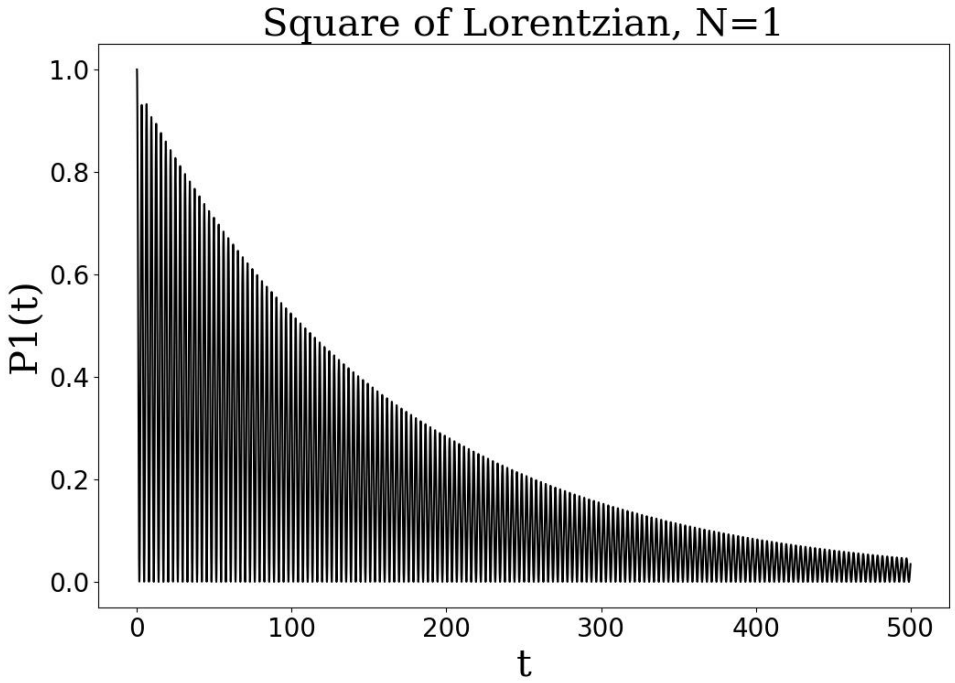

FIGURE 3.3: Dynamics of the populations of a qubit connected to a square of Lorentzian reservoir for $c_1(0) = 1$,$\Gamma = 0.3$, $g = 1$, $J = 1$.

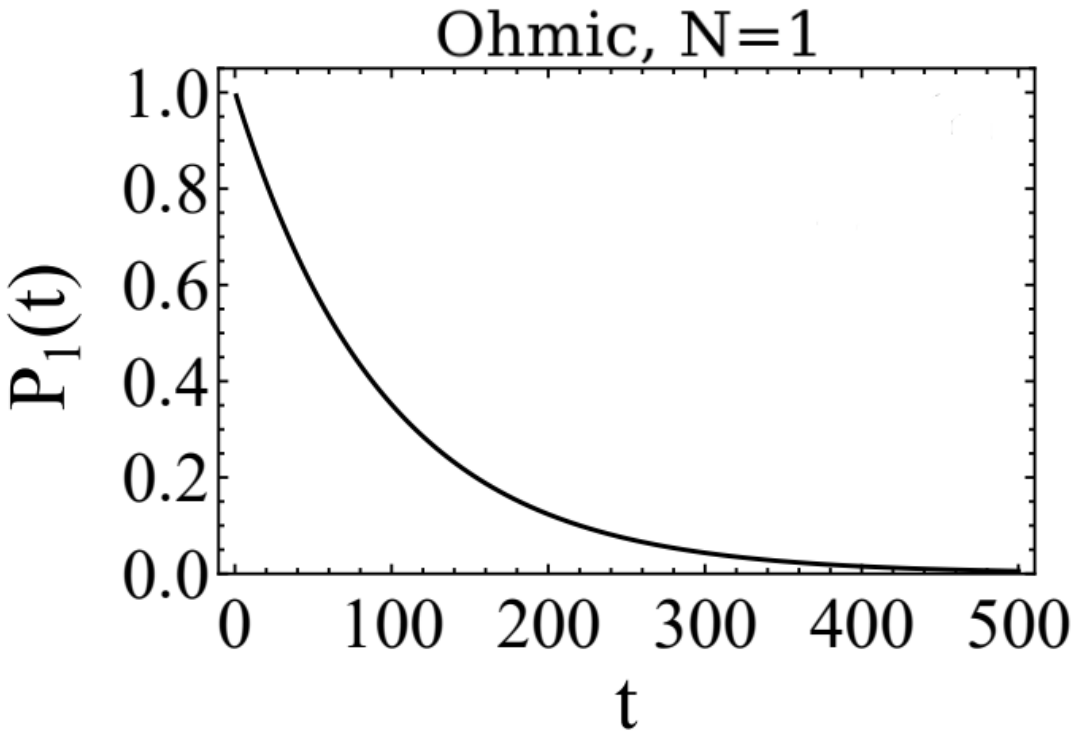

FIGURE 3.4: Dynamics of the populations of a qubit connected to an Ohmic reservoir for $c_1(0) = 1$, $S = 1.5$, $g = 1$,$\omega_c = 8$,$\omega_{eg} = 10$, $J = 1$

In Figures 3.1-3.4, we present the time dynamics of the survival probability of a single qubit excitation across different types of reservoirs. Specifically, we investigate the scenarios involving Markovian, Lorentzian, Lorentzian squared and Ohmic reservoirs, with the parameters for each non-Markovian reservoir set according to the previously described specifications. In Fig. 3.1 and 3.2, we can see that the Markovian and Lorentzian for N=1 are in match with what we predict in equations (3.3) and (3.10). The spectral densities associated with Lorentzian and Lorentzian squared profiles generally induce rapid oscillations in the dynamics of the single-qubit excitation survival, indicating the transfer of excitation between the qubit and its environment within finite time intervals. These oscillations in Figures 3.2 and 3.3, are also evidence of the non-Markovian character of the Lorentzian and Lorentzian squared reservoirs and can be interpreted as a backflow of information from the reservoir to the system. The heightened frequency of these oscillations is ascribed to a substantial coupling strength g in relation to the widths Γ of the Lorentzian and Lorentzian squared distributions. A reduction in g results in a corresponding decrease in the oscillation frequency. It is noteworthy that the Markovian limit can be approximated by increasing Γ, while simultaneously maintaining the ratio $\frac{g^2}{\Gamma}$ at a constant value. On the other hand, the Ohmic spectral distribution typically exhibits a broader profile compared to Lorentzian and Lorentzian squared distributions. This broader profile leads to a qubit excitation survival probability that more closely resembles the survival probability observed in the Markovian case as shown in Fig. 3.4. This is an expected result as it has been shown by Lambropoulos and Mouloudakis that the effect of a super-Ohmic reservoir resembles an almost Markovian reservoir.

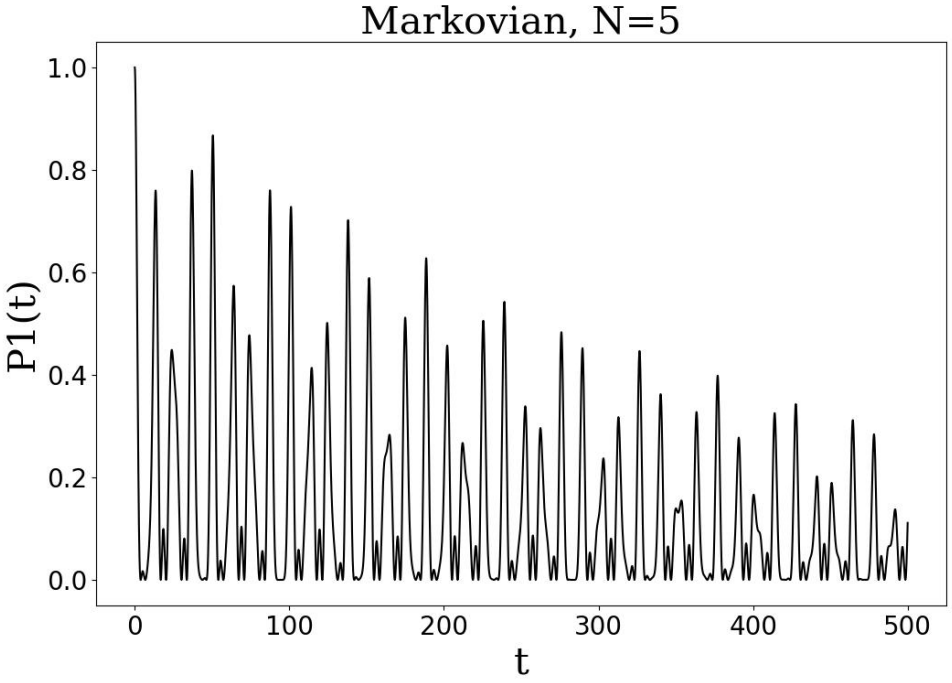

FIGURE 3.5: Dynamics of the populations of the first qubit of a 5-qubit chain connected to a Markovian reservoir for $c_1(0) = 1$,$\Gamma = 0.01$, $J = 1$.

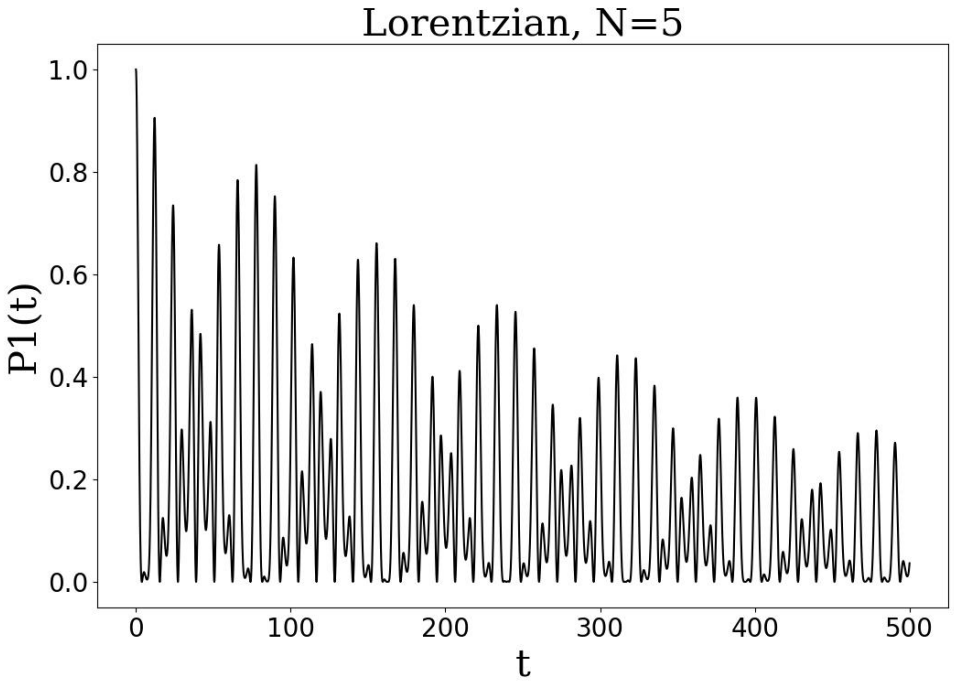

FIGURE 3.6: Population dynamics of the first qubit of a 5-qubit chain connected to a Lorentzian reservoir for $c_1(0) = 1$,$\Gamma = 0.03, g = 1, J = 1$.

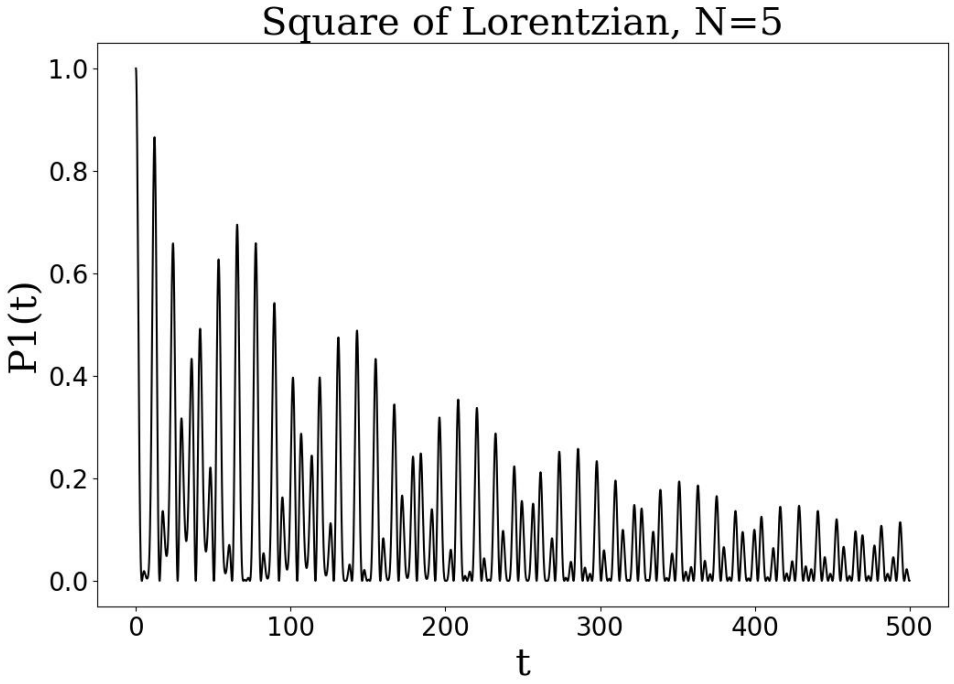

FIGURE 3.7: Population dynamics of the first qubit of a 5-qubit chain connected to a Square of Lorentzian reservoir for $c_1(0) = 1$,$\Gamma = 0.3, g = 1, J = 1$.

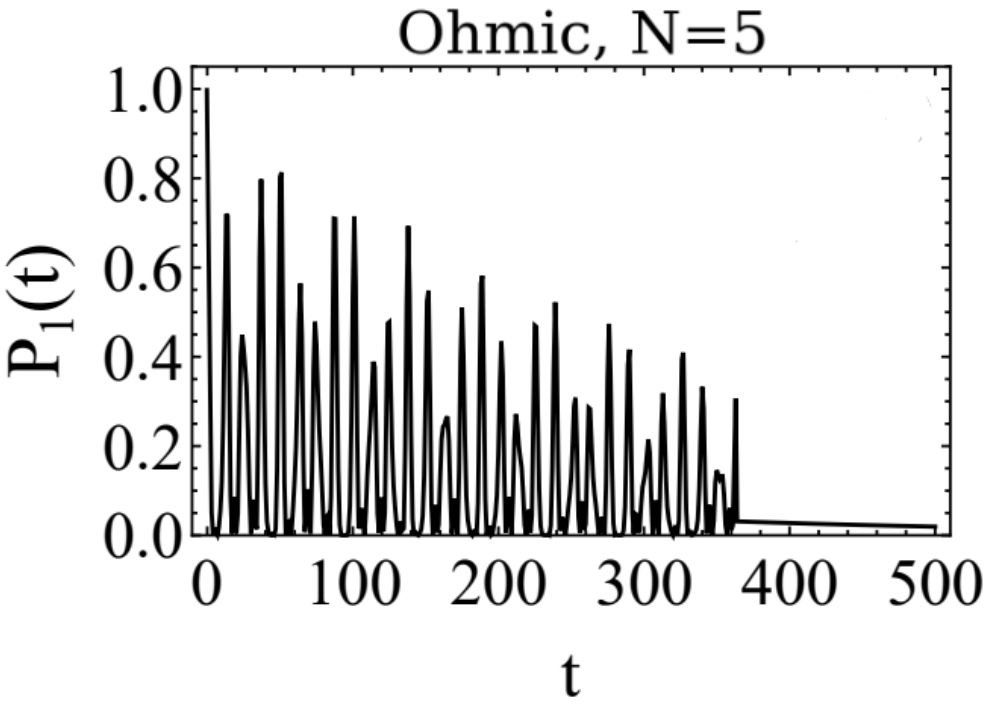

FIGURE 3.8: Population dynamics of the first qubit of a 5-qubit chain connected to an Ohmic reservoir for $c_1(0) = 1, S = 1.5, g = 1, \omega_c = 8, \omega_{eg} = 10, J = 1$

The reason we started with the simplistic 1-qubit system, is for it to serve as a calibration for the measures of QSD in characterising non-Markovianity. In Figures 3.5-3.8, we study the more realistic situation of a 5-qubit chain invlonving qubit-qubit interaction. In a configuration of this nature, the pivotal parameter is J, as it controls the inter-qubit communication which is typically a predominant factor in practical applications. To adhere to a realistic scenario, we opt for a Markovian damping rate Γ significantly smaller than J. The chosen parameters for the non-Markovian reservoirs remain consistent with the ones for the 1-qubit system, ensuring that the initial excitation for the first qubit decays on a timescale approximately equal for all reservoirs.

Initially, we compute the time evolution of the excitation probability for the first qubit across all considered reservoirs. A notable distinction between the single-qubit dynamics and the dynamics of the first qubit excitation in the 5-qubit chain is the emergence of oscillations in the latter's dynamics, signifying the exchange of population among the qubits in the chain. In Figures 3.6, 3.7 we can see that for the Lorentzian and Lorentzian squared reservoirs these oscillations overlay those occurring between the last qubit and the reservoir.

For the Markovian scenario(Fig. 3.5), the oscillations stem exclusively from the coupling between the qubits. Lastly, in the Ohmic damped case, the dynamics of the first qubit population(Fig. 3.8) closely resembles that of the Markovian-damped chain, with the noteworthy exception that the oscillations unexpectedly collapse after a finite time, a behavior also documented in prior studies involving qubits coupled to Ohmic reservoirs (Mouloudakis, Ilias, and Lambropoulos, 2022, Abdi and Plenio, 2018).

3.2 QSD Results

In this section, we present numerical results of the time dynamics of the various distance measures between Markovian and non-Markovian reservoirs. At the end of the section we analyze the results and compare the three distance measures.

As stated before, we begin our analysis by examining the simplest scenario: a single qubit interacting with various non-Markovian reservoirs. These findings provide a foundational reference. In our codes, we have solved the problem in its most general form meaning that N is a modifiable parameter. After establishing the measures of QSD for characterizing non-Markovianity in this basic setup, we proceed to investigate the role of non-Markovianity in a more complex and realistic context, specifically a chain involving qubit-qubit interactions. For a detailed quantitative analysis, we select a system of five qubits arranged in an XX chain with nearest-neighbor coupling J. The central question is how the non-Markovianity of the reservoir influences the exchange of excitation between the qubits, as manifested by the evolution of QSD between the Markovian and various non-Markovian reservoirs.

3.2.1 N=1 case

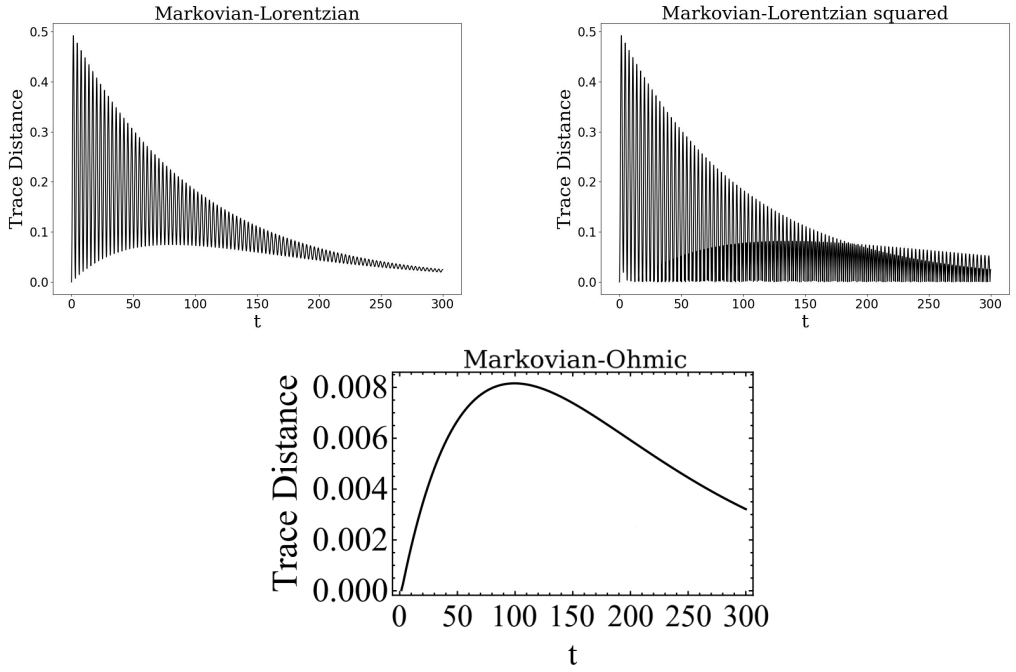

FIGURE 3.9: Trace Distance between the Markovian and the non-Markovian system using three types of non-Markovian reservoirs in the single-qubit case. The parameters used in each case are: Markovian reservoir with $\Gamma_M = 0.01$, Lorentzian reservoir with g=1, $\Gamma = 0.03$ and $\Delta_c = 0$, Lorentzian squared reservoir with g=1 , $\Gamma = 0.3$ and $\Delta_c = 0$, Ohmic reservoir with g=1, S=1.5, $\omega_c = 8$ and qubit frequency $\omega_{eg} = 10$.

In Fig 3.9 we study the trace distance between a single qubit connected to a Markovian reservoir and a single qubit connected to a non-Markovian reservoir. The parameters used are the same we used for the study of the population dynamics in subsection 3.1.2. The trace distance as we know assumes values between 0 and 1,

0 meaning there is no distinguishability between the states. It is therefore expected from the trace distance to be 0 at t=0 because the reservoirs have not yet started to affect the qubit, meaning that we are essentially comparing between two identical qubits. Adding to that, we also expect from the trace distance to be zero for $t \to \infty$ as the population will eventually be lost to the reservoir meaning that we will be comparing two qubits with no excitation in them.

The trace distance in the Markovian-Lorentzian case, shows rapid oscillations between two bounds that vary over time. Initially, the upper bound is at its peak and gradually decreases to zero, while the lower bound starts low, increases to a peak, and then decreases, eventually merging with the upper bound and tending to zero for $t \to \infty$. Similarly, the trace distance dynamics between the Markovian and Lorentzian-squared display rapid oscillations following a comparable pattern to the Markovian-Lorentzian case. However, the lower bound in this scenario can reach zero at specific times, indicating moments when the Lorentzian-squared damped system closely resembles the Markovian-damped system. These oscillations in both the Lorentzian and Lorentzian squared cases, indicate a swift exchange of excitation between the qubit and the non-Markovian reservoirs. Unlike the previous cases, the trace distance in the Markovian-Ohmic case does not exhibit oscillations, reaches a maximum at a finite time, and then decreases, with overall values significantly lower than those in the Markovian-Lorentzian and Markovian-Lorentzian squared cases. Consequently, it can be concluded that, under the given parameter conditions, the Ohmic-damped single qubit system demonstrates the lowest degree of non-Markovianity.

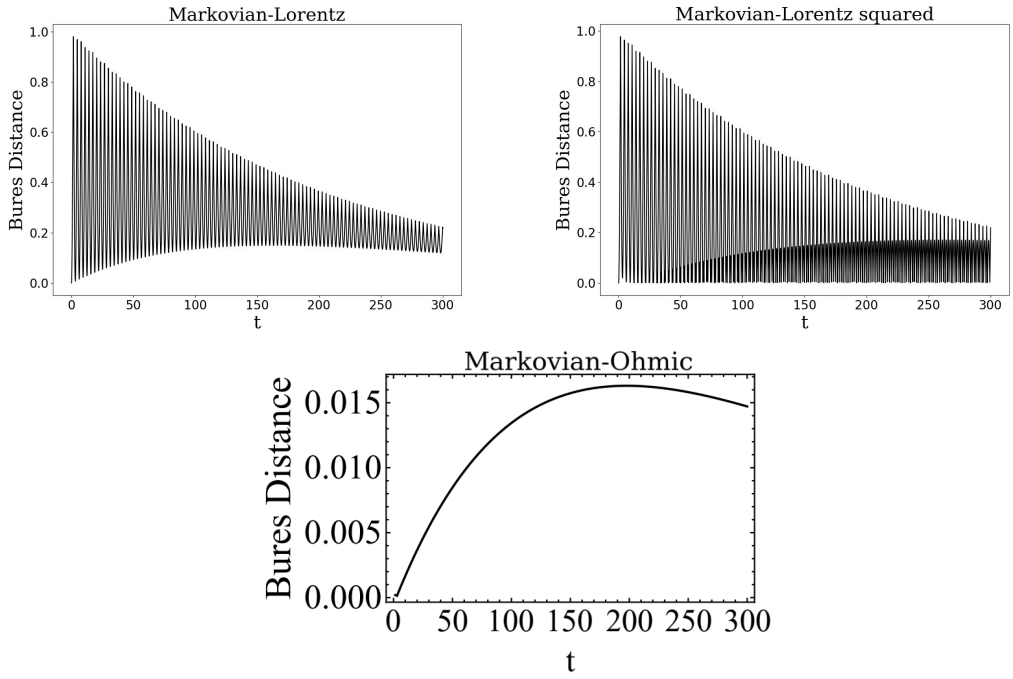

FIGURE 3.10: Bures Distance between the Markovian and the non-Markovian system using three types of non-Markovian reservoirs in the single-qubit case. The parameters used in each case are: Markovian reservoir with $\Gamma_M = 0.01$, Lorentzian reservoir with g=1, $\Gamma = 0.03$ and $\Delta_c = 0$, Lorentzian squared reservoir with g=1 , $\Gamma = 0.3$ and $\Delta_c = 0$, Ohmic reservoir with g=1, S=1.5, $\omega_c = 8$ and qubit frequency $\omega_{eg} = 10$.

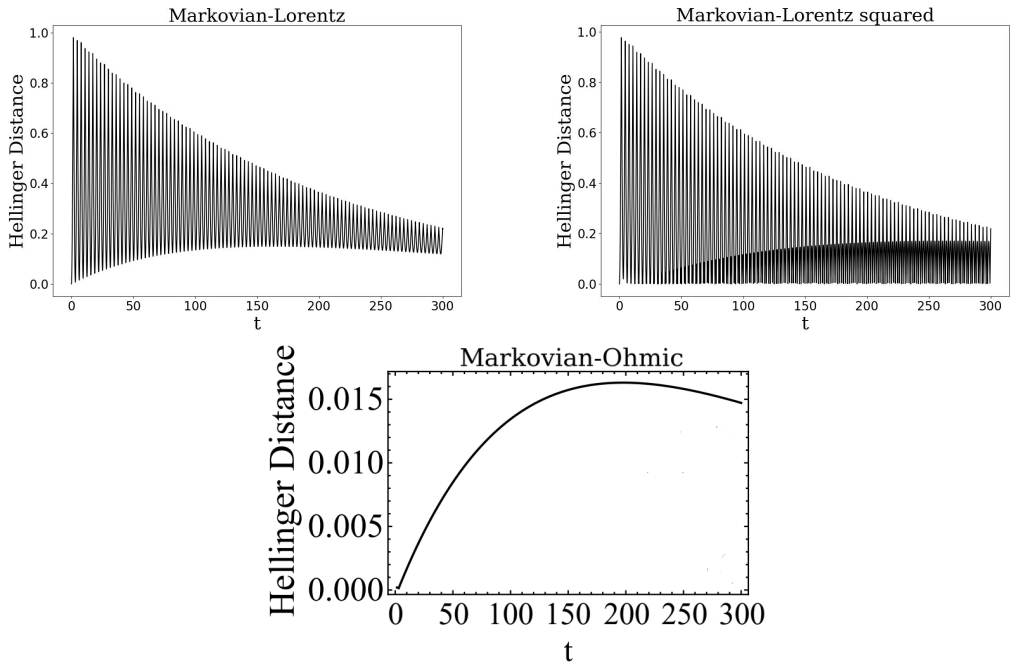

FIGURE 3.11: Hellinger Distance between the Markovian and the non-Markovian system using three types of non-Markovian reservoirs in the single-qubit case. The parameters used in each case are: Markovian reservoir with $\Gamma_M = 0.01$, Lorentzian reservoir with g=1, $\Gamma = 0.03$ and $\Delta_c = 0$, Lorentzian squared reservoir with g=1 , $\Gamma = 0.3$ and $\Delta_c = 0$, Ohmic reservoir with g=1, S=1.5, $\omega_c = 8$ and qubit frequency $\omega_{eg} = 10$.

In Fig 3.10 and 3.11 we present results using the Bures and the Hellinger metric respectively. We can clearly see that both QSD measures display nearly identical behaviour with the only difference being that the Bures and Hellinger measures exhibit a generally slower decay of QSD compared to the Trace distance. Additionally, the Lorentzian and Lorentzian squared oscillations in QSD obtained from these two measures are attenuated more gradually than those in the Trace distance. The Ohmic case follows a similar pattern, yielding higher QSD values and a significantly slower progression toward the anticipated value of 0 for all reservoirs and measures. In summary, for all three non-Markovian reservoirs in the single qubit scenario, the Trace distance demonstrates a more rapid decline in non-Markovianity compared to the Hellinger and Bures measures. It is noteworthy that despite the substantial formal differences in the expressions for the Hellinger and Bures QSD, they result in nearly identical dynamics, indicating the same degree of non-Markovianity.

3.2.2 N=5 case

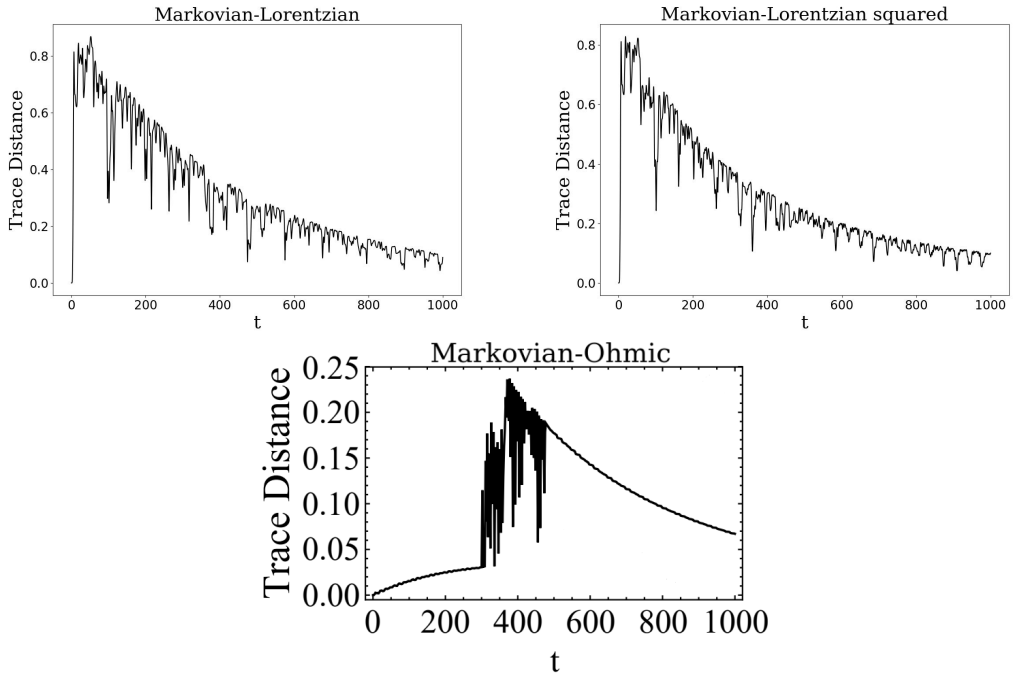

FIGURE 3.12: Trace Distance between the Markovian and the non-Markovian system using three types of non-Markovian reservoirs for a qubit chain of N=5 and qubit-qubit coupling J=1. The parameters used in each case are: Markovian reservoir with $\Gamma_M = 0.01$, Lorentzian reservoir with g=1, $\Gamma = 0.03$ and $\Delta_c = 0$, Lorentzian squared reservoir with g=1 , $\Gamma = 0.3$ and $\Delta_c = 0$, Ohmic reservoir with g=1, S=1.5, $\omega_c = 8$ and qubit frequency $\omega_{eg} = 10$.

In Fig 3.12 we examine the Trace distance between a 5-qubit chain connected to a Markovian reservoir and a 5-qubit chain connected to a non-Markovian reservoir. The parameters used are again the same we used for the study of the population dynamics in subsection 3.1.2.

First, we observe that all of the Trace distance measures have decay time scales that are longer than the corresponding time scales in the single-qubit case. Given that the excitation is now dispersed throughout the entire chain and that it takes longer for populations to be lost in the reservoir, this behavior was expected. Simultaneously, the Trace distance values are generally higher than the single-qubit corresponding values, suggesting that the number of qubits in the open system influences its degree of Non-Markovianity.Overall, it is observed that the behavior of the Markovian-Lorentzian and Markovian-Lorentzian-squared Trace distance is similar.When considering the Ohmic-damped chain, a phenomenon that is quite intriguing can be seen in the dynamic behavior of the Trace distance. The dynamics of the Markovian-Ohmic measurements under consideration exhibit a complex phenomenon, in contrast to the single-qubit case, due to the interplay between qubit-qubit and qubit-Ohmic reservoir interactions. With the distance being zero at t = 0 and gradually increasing afterward, the dynamics are initially smooth. Occasionally, though, they will abruptly alter and display rapid oscillations. Only within a time

window that is consistent for all QSD measures, as we show in the graphs tha follow, taken into consideration do these fast oscillations occur. The dynamics smooth out after that time window, with the distance gradually decaying to zero.

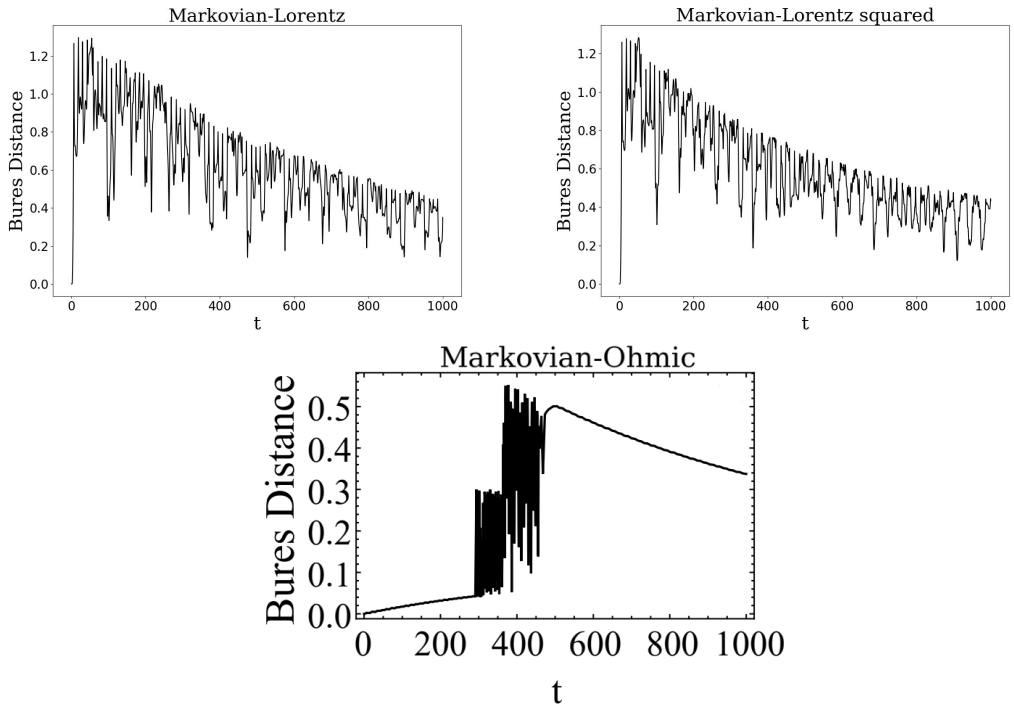

FIGURE 3.13: Bures Distance between the Markovian and the non-Markovian system using three types of non-Markovian reservoirs for a qubit chain of N=5 and qubit-qubit coupling J=1. The parameters used in each case are: Markovian reservoir with $\Gamma_M = 0.01$, Lorentzian reservoir with g=1, $\Gamma = 0.03$ and $\Delta_c = 0$, Lorentzian squared reservoir with g=1 , $\Gamma = 0.3$ and $\Delta_c = 0$, Ohmic reservoir with g=1, S=1.5, $\omega_c = 8$ and qubit frequency $\omega_{eg} = 10$.

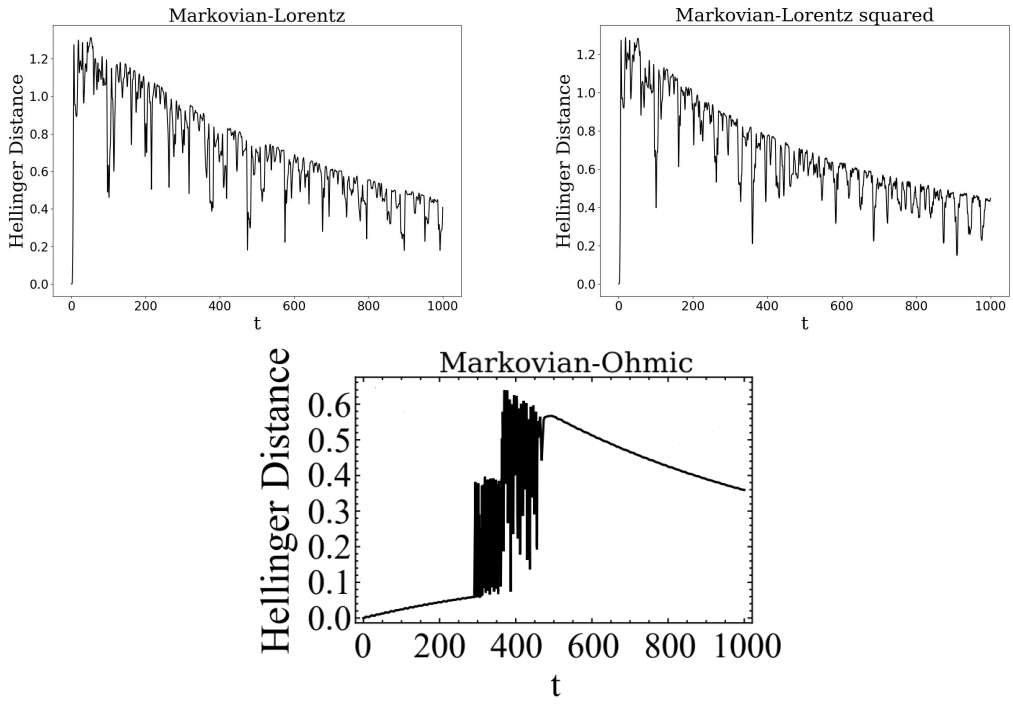

FIGURE 3.14: Hellinger Distance between the Markovian and the non-Markovian system using three types of non-Markovian reservoirs for a qubit chain of N=5 and qubit-qubit coupling J=1. The parameters used in each case are: Markovian reservoir with $\Gamma_M = 0.01$, Lorentzian reservoir with g=1, $\Gamma = 0.03$ and $\Delta_c = 0$, Lorentzian squared reservoir with g=1 , $\Gamma = 0.3$ and $\Delta_c = 0$, Ohmic reservoir with g=1, S=1.5, $\omega_c = 8$ and qubit frequency $\omega_{eg} = 10$.

In Fig 3.13 and 3.14 we present results using the Bures and the Hellinger metric respectively. As in the single-qubit case, both QSD measures display similar behaviour with the Trace distance with the difference being that the decay of the QSD is slower. Adding to that, we can see that the time window, in which the Markovian-Ohmic suddenly alter into rapid oscillations, is the same for all QSD measures.

In conclusion, it is found that the qubit-qubit interaction increases the degree of Non-Markovianity found in all QSD measures. On the other hand, the reservoir's non-Markovian properties could be seen as improving the excitation storage in the chain.

3.3 Entanglement

In this section, we study the time evolution of the entanglement as affected by various reservoirs. For that purpose, we consider a 6-qubit chain, with the qubits labelled as 1,2,3,4,5 and 6. As an initial condition, we set qubits 1 and 2 maximally entangled. Qubits 3 and 4 are taken coupled to two identical reservoirs. The question then is the time evolution of the entanglement as it propagates to qubits 5 and 6, under various reservoirs coupled to qubits 3 and 4. As has been shown in Mouloudakis and Lambropoulos, 2023, two interacting qubits coupled to identcal reservoirs, are equivalent to an arbitrary number of qubits all of which are coupled to the same reservoir, with proper scaling. Therefore, this arrangement is equivalent to the propagation of the entanglement of two qubits to another pair of distant qubits, via a chain of an arbitrary number of interacting qubits coupled to identical environments (reservoirs). In different words, we study the propagation of entanglement through a lossy chain of qubits. The entanglement of two qubits is characterized quantitatively by the concurrence. In order to explore quantitatively the transfer of entanglement through the lossy chain, we calculate the time evolution of the concurrence, under coupling of the intermediate qubits to various reservoirs. The concurrence of two qubits is given by the expression:

$$C(t) = 2|c_1(t)c_2^*(t)|$$

with values ranging from 0 (lowest) and 1 (maximum entanglement). This metric is frequently used to measure entanglement between edge qubits in qubit-chains, especially when they begin as unentangled and result in a steady state entanglement after some time. In that case we have what often referred to as the long distance entanglement generation which is important for quantum computer applications.

In the graphs that follow, we present results for the time dynamics of the populations of the edge qubits and the time dynamics of their concurrence.

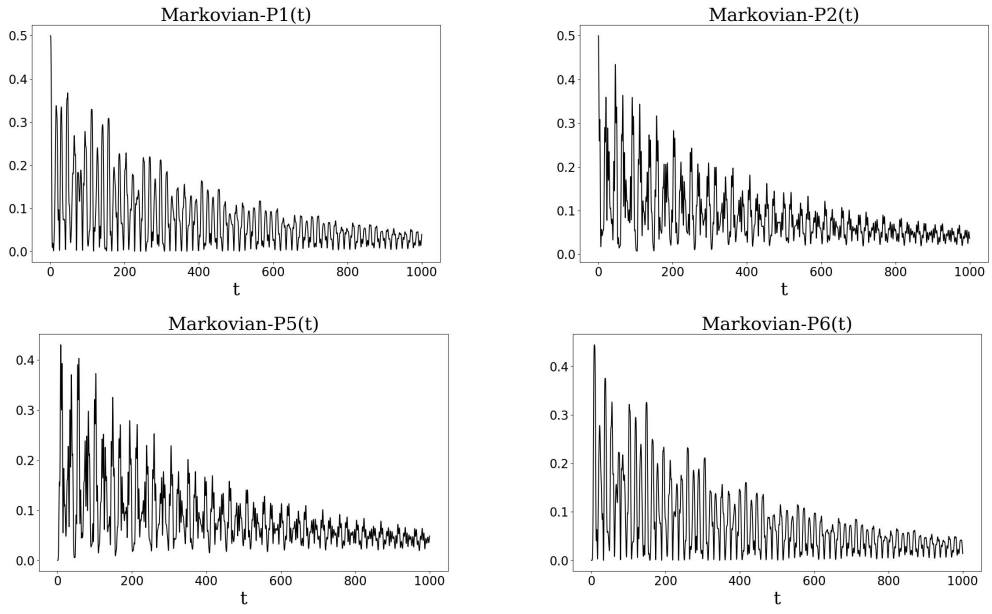

FIGURE 3.15: Population dynamics of the edge qubits of a 6 qubit-chain with each of the middle qubits connected to an identical Markovian reservoir for $c_1(0) = 1/\sqrt{2}, c_2(0) = 1/\sqrt{2}, \Gamma = 0.01, J = 1$.

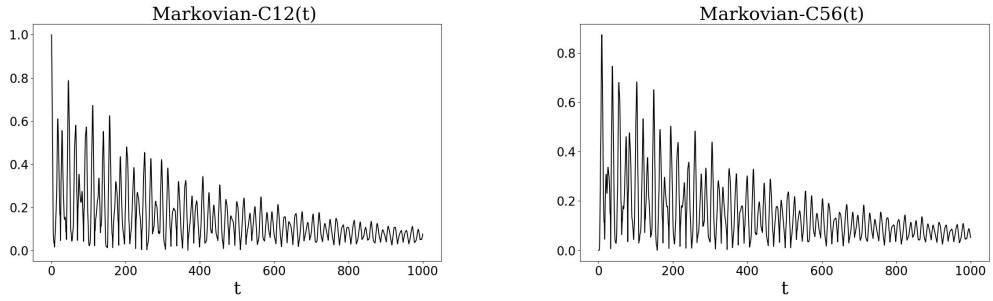

FIGURE 3.16: Time dynamics of the edge qubits concurrence in a 6 qubit-chain with each of the middle qubits connected to an identical Markovian reservoir for $c_1(0) = 1/\sqrt{2}, c_2(0) = 1/\sqrt{2}, \Gamma = 0.01, J = 1$.

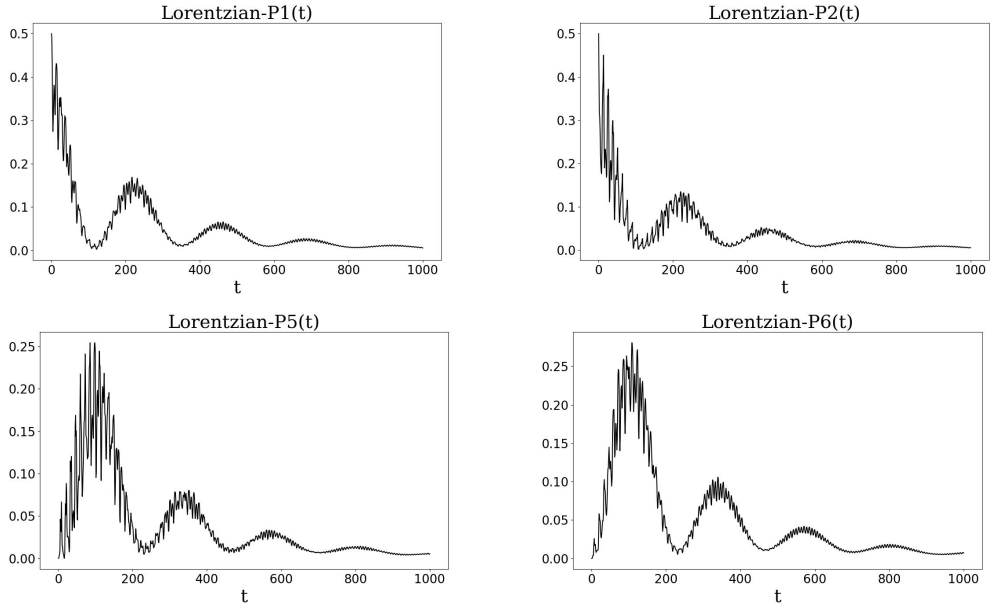

FIGURE 3.17: Population dynamics of the edge qubits of a 6 qubit-chain with each of the middle qubits connected to an identical Lorentzian reservoir for $c_1(0) = 1/\sqrt{2}, c_2(0) = 1/\sqrt{2}, \Gamma = 0.03, g = 1, J = 1$.

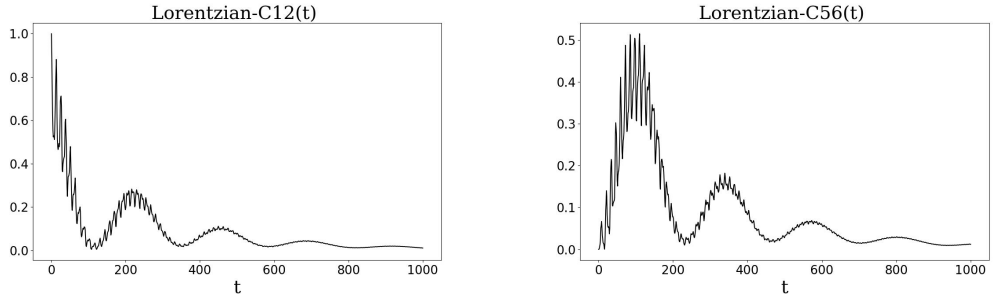

FIGURE 3.18: Time dynamics of the edge qubits concurrence in a 6 qubit-chain with each of the middle qubits connected to an identical Lorentzian reservoir for $c_1(0) = 1/\sqrt{2}, c_2(0) = 1/\sqrt{2}, \Gamma = 0.03, g = 1, J = 1$.

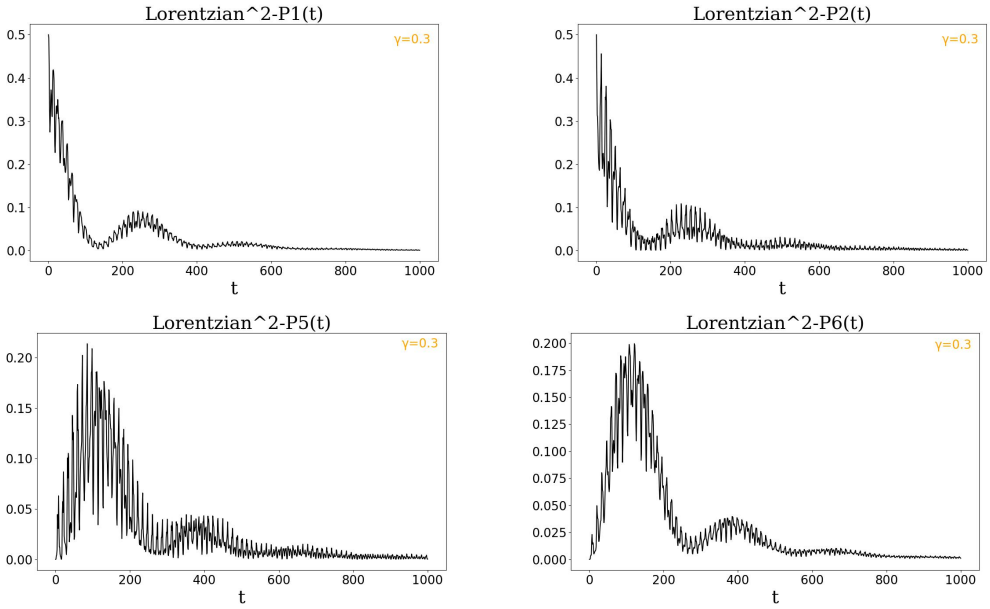

FIGURE 3.19: Population dynamics of the edge qubits of a 6 qubit-chain with each of the middle qubits connected to an identical Lorentzian squared reservoir for $c_1(0) = 1/\sqrt{2}, c_2(0) = 1/\sqrt{2}, \Gamma = 0.3, g = 1, J = 1$.

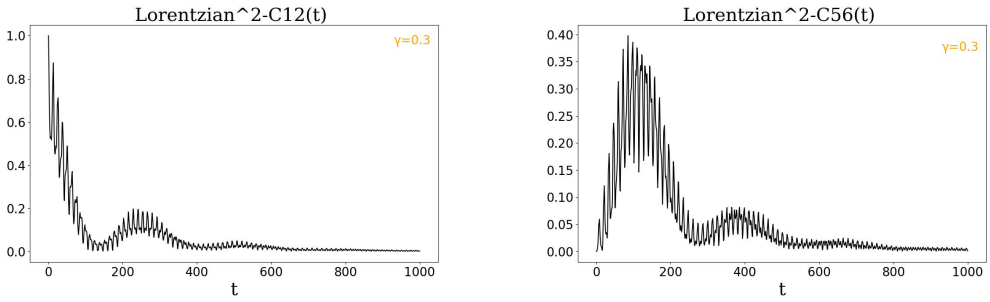

FIGURE 3.20: Time dynamics of the edge qubits concurrence in a 6 qubit-chain with each of the middle qubits connected to an identical Lorentzian squared reservoir for $c_1(0) = 1/\sqrt{2}, c_2(0) = 1/\sqrt{2}, \Gamma = 0.3, g = 1, J = 1$.

In Fig. 3.15, we present the population dynamics of the edge qubits in a 6-qubit chain, with two Markovian reservoirs connected to each of the middle qubits. The initial conditions are set for maximum entanglement between the first two qubits. The results indicate that the populations do not preserve any entanglement, exhibiting the typical Markovian behavior as demonstrated in previous sections. This is further corroborated by Fig. 3.16, where the concurrence of the edge qubits gradually decays to zero.

In Figs. 3.17-3.20, we show the population dynamics and concurrence of the edge qubits in a 6-qubit chain with two Lorentzian reservoirs (Figs. 3.17-3.18) and two Lorentzian squared reservoirs (Figs. 3.19-3.20) connected to each of the middle qubits. For both cases, the initial conditions are set to maximum entanglement between the first two qubits, with decay parameters $\Gamma_1 = 0.03$ for the Lorentzian and $\Gamma_2 = 0.3$ for the Lorentzian squared. The populations of the edge qubits in both scenarios exhibit the typical oscillatory behavior associated with Lorentzian and

Lorentzian squared damped cases. However, the populations decay faster than previously observed, which is expected due to the introduction of two reservoirs in the middle of the chain, reducing the space for population travel and resulting in faster decay. Additionally, the Lorentzian squared decay occurs slightly faster than the Lorentzian, consistent with it being a more pronounced version of the Lorentzian. The concurrence of the edge qubits in both cases starts at maximum entanglement and rapidly decays to zero, indicating no preservation of entanglement.

So far, our calculations have set the parameter Γ for all reservoirs to ensure that the half-life of the excitation of the first qubit is approximately the same. While this is a reasonable standard, it is also worth exploring what occurs if we set the parameters identically, particularly in the Lorentzian and Lorentzian squared cases. To accurately compare the Lorentzian with the Lorentzian squared reservoir, we should use the same input parameters to elucidate their differences.

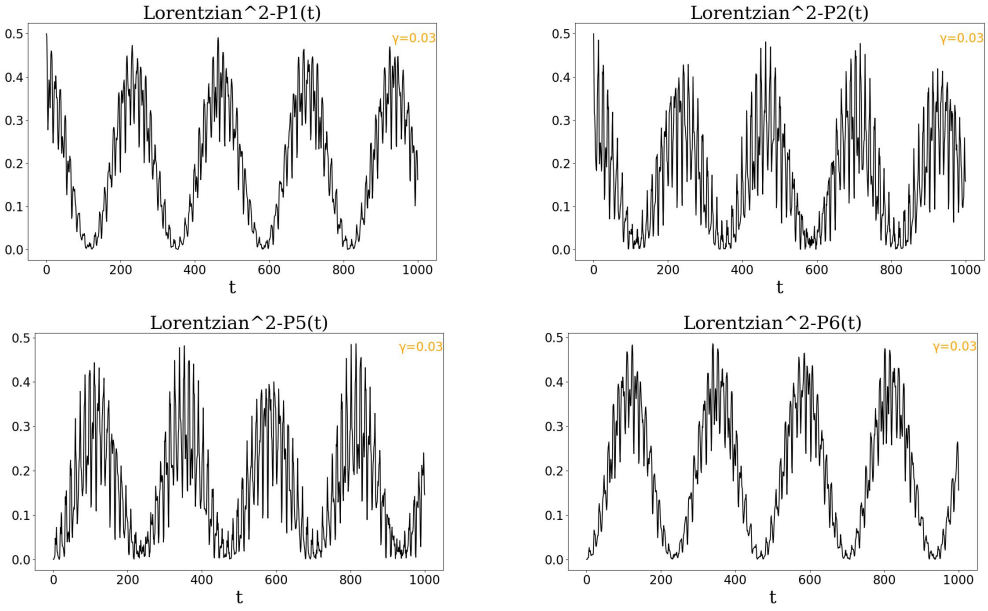

FIGURE 3.21: Population dynamics of the edge qubits of a 6 qubit-chain with each of the middle qubits connected to an identical Lorentzian squared reservoir for $c_1(0) = 1/\sqrt{2}, c_2(0) = 1/\sqrt{2}, \Gamma = 0.03, g = 1, J = 1$.

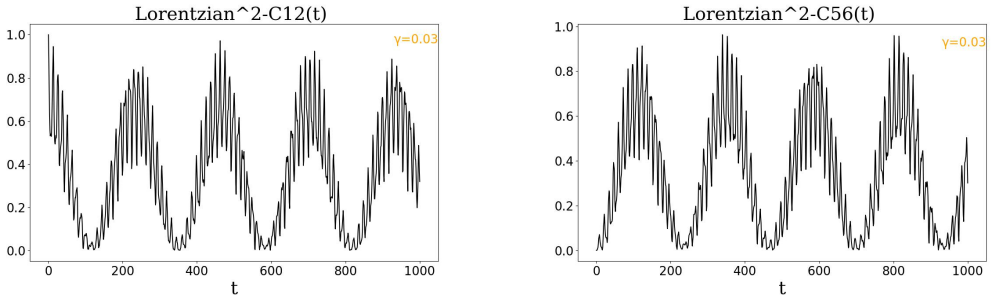

FIGURE 3.22: Time dynamics of the edge qubits concurrence in a 6 qubit-chain with each of the middle qubits connected to an identical Lorentzian squared reservoir for $c_1(0) = 1/\sqrt{2}, c_2(0) = 1/\sqrt{2}, \Gamma = 0.03, g = 1, J = 1$.

In Fig. 3.21, we have set the decay parameter for the Lorentzian squared case to $\Gamma = 0.03$. The results are compelling, as there is practically no decay of the excitations. The populations remain essentially frozen within the chain, oscillating between the edge qubits.

In Fig. 3.22, we present the time dynamics of the concurrence of the edge qubits. The concurrence oscillates between zero and one with negligible decay. When qubits one and two exhibit maximum entanglement, indicated by a concurrence value of one, qubits five and six show zero concurrence, and vice versa. This indicates the establishment of a steady state of transfer of entanglement. Given the significance of this finding, the next chapter will explore the dynamics of the Lorentzian squared for lower values of Γ.

Chapter 4

A more thorough examination of the Lorentzian squared

4.1 Population dynamics for $\Gamma = 0.03$

The population dynamics of spin chains coupled to Lorentzian and Ohmic reservoirs have been studied thoroughly by Mouloudakis and Labropoulos [reference]. The Lorentzian squared on the other hand is a reservoir that, to our knowlegde, has never been examined in a realistic model like ours. The purpose of this section, is to study the reservoir's behavior when changing the variables of the problem. We also look at the sum of populations, in order to determine what conditions result in the population trapping. Note that, in all our calculations, we adopt the value J=1 for the strength of the interaction between neighboring qubits, as a reference value for the comparison with the other couplings entering the formalism.

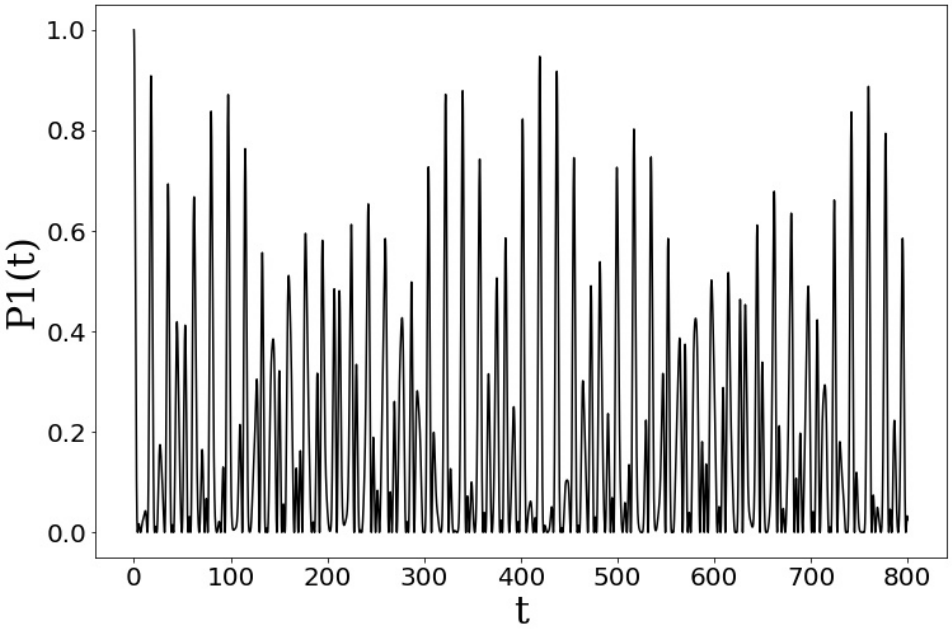

FIGURE 4.1: Population dynamics of the first qubit of a 5-qubit chain connected to a Square of Lorentzian reservoir for $c_1(0) = 1$, $\Gamma = 0.03$, g=0.3, J=1 .

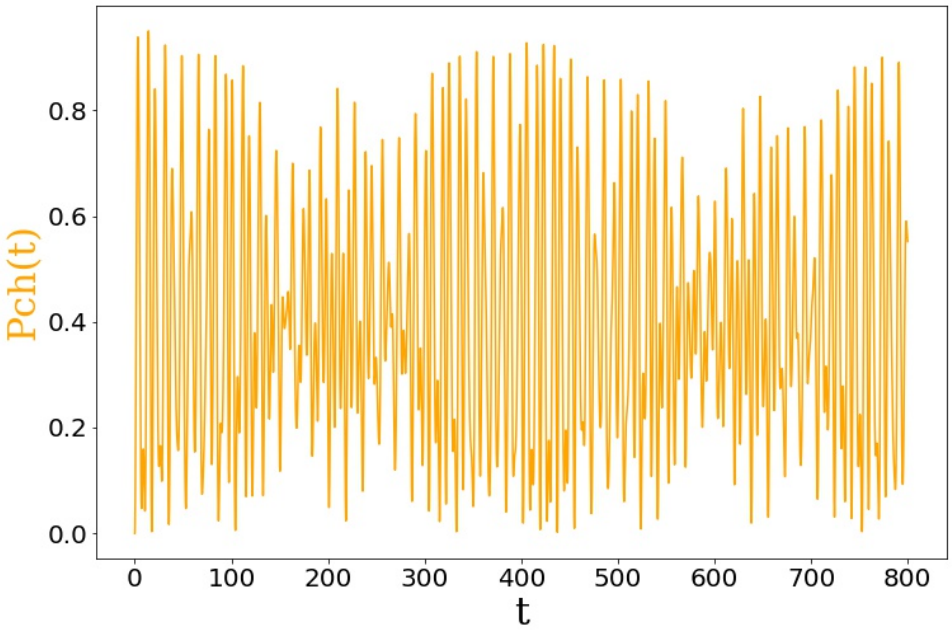

FIGURE 4.2: Population dynamics of the channel qubits of a 5-qubit chain connected to a Square of Lorentzian reservoir for $c_1(0) = 1$, $\Gamma = 0.03$, g=0.3, J=1 .

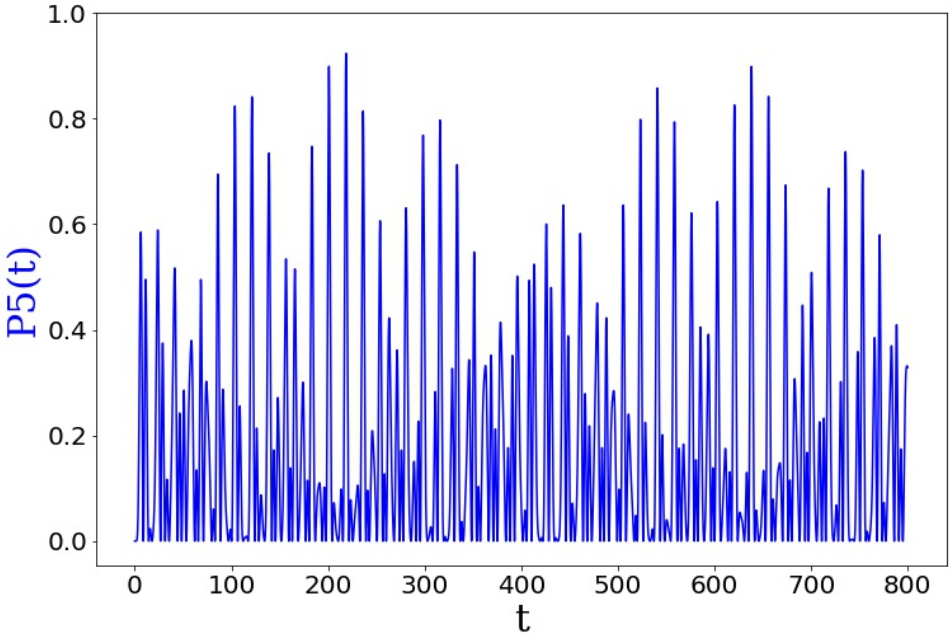

FIGURE 4.3: Population dynamics of the last qubit of a 5-qubit chain connected to a Square of Lorentzian reservoir for $c_1(0) = 1$, $\Gamma = 0.03$, g=0.3, J=1 .

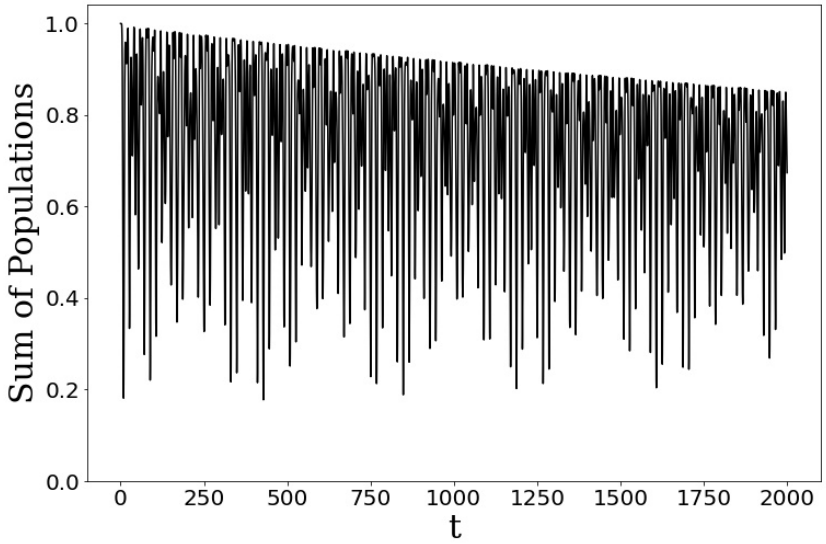

FIGURE 4.4: Sum of populations of a 5-qubit chain connected to a Square of Lorentzian reservoir for $c_1(0) = 1$, $\Gamma = 0.03$, g=0.3, J=1 .

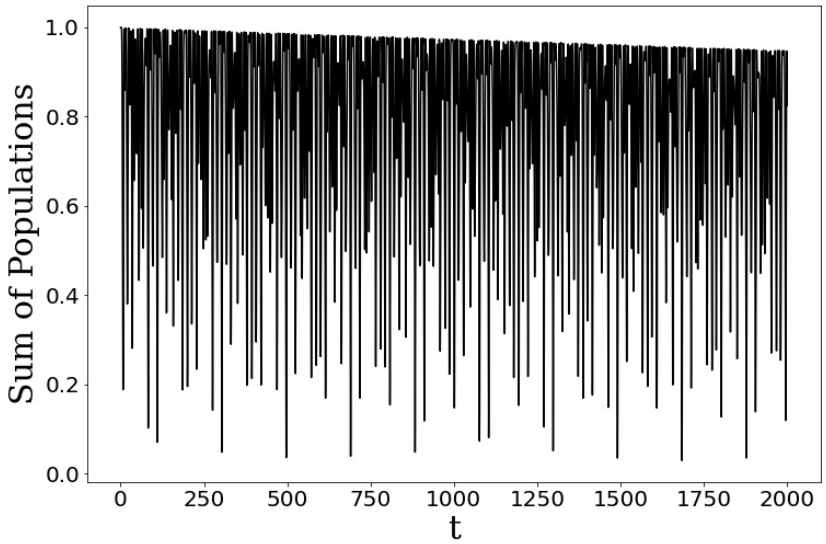

FIGURE 4.5: Sum of populations of a 5-qubit chain connected to a Square of Lorentzian reservoir for $c_1(0) = 1$, $\Gamma = 0.03$, g=0.6, J=1 .

In Fig 4.1-4.5 we study the dynamics of the population of the edge as well as the intermediate qubits in the g < J case. For the intermediate qubits, we adopt the term "channel qubits", which is frequently used in quantum information protocols and represents the sum of populations of all except the 2 edge qubits. In Figures 4.1-4.3, we observe oscillations in the edge and channel qubit populations corresponding to the spreading of the initial excitation over the whole chain and the backflow from the reservoir. The sum of populations of the chain for g=0.3 is depicted in Fig 4.4. As we can see the population will eventually, though very slowly, be lost due to the environmental dissipation. This is a finding that is characteristic of the square of

Lorentzian reservoir, as none of the other reservoirs that we have studied produce such slow dissipation to the environment. Moreover, when raising the value of g while staying in the g < J regime, the total population of chain decays even slower as shown in Fig 4.5. When raising the value of g, we also observe oscillations of higher amplitude in the total population of the chain. This means that more population is exchanged back and forth between the reservoir and the chain, suggesting a more non-Markovian behaviour.

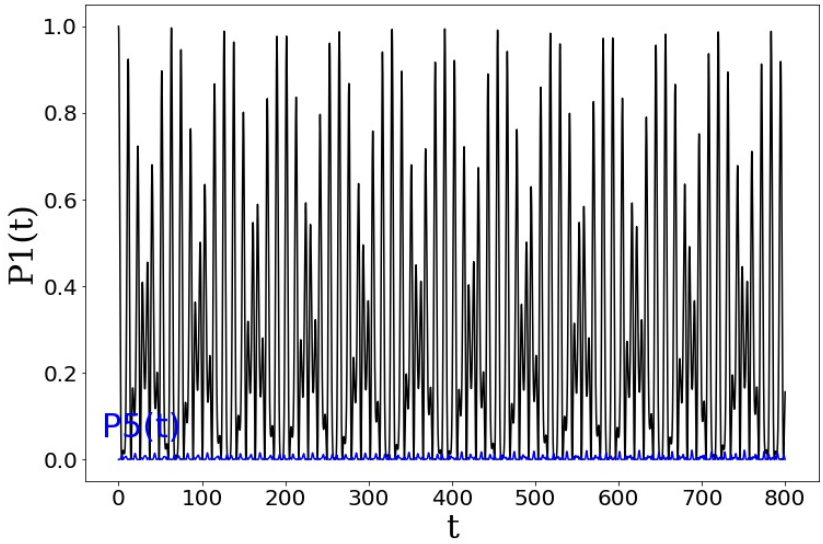

FIGURE 4.6: Population dynamics of the first and last qubit of a 5-qubit chain connected to a Square of Lorentzian reservoir for $c_1(0) = 1, \Gamma = 0.03$, g=1.5, J=1 .

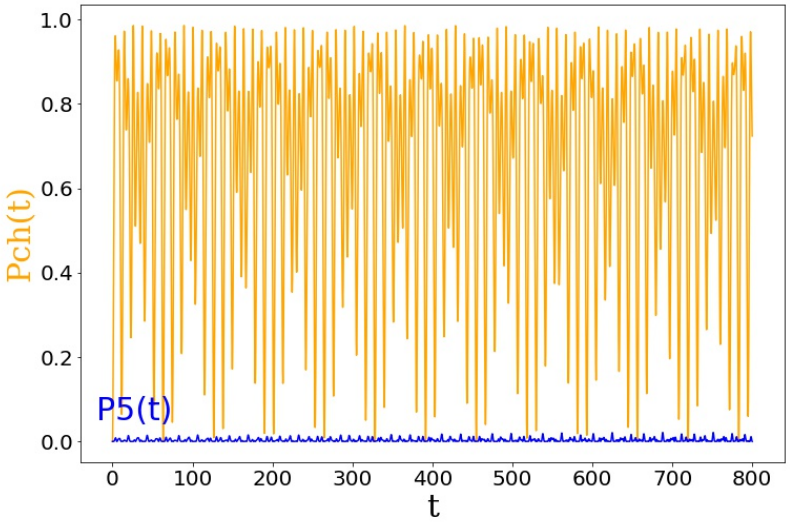

FIGURE 4.7: Population dynamics of the channel and last qubit of a 5-qubit chain connected to a Square of Lorentzian reservoir for $c_1(0) = 1, \Gamma = 0.03$, g=1.5, J=1 .

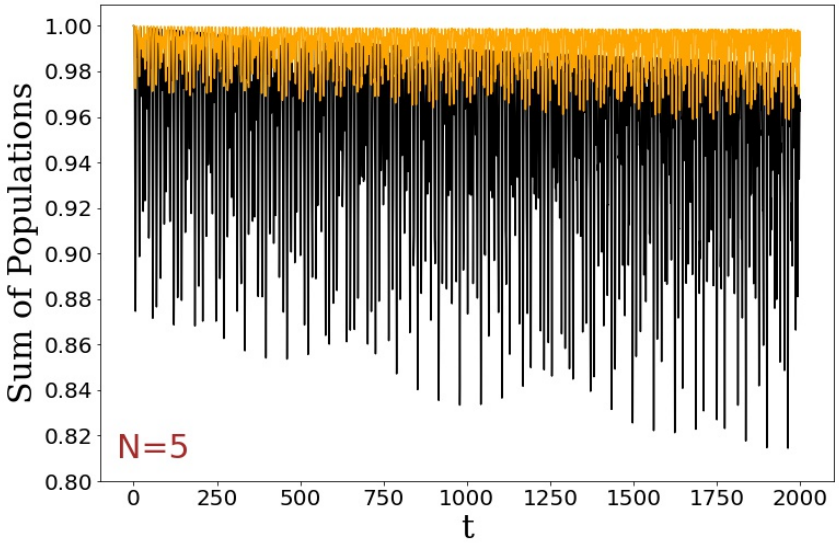

FIGURE 4.8: Sum of populations of a 5-qubit chain connected to a Square of Lorentzian reservoir for $c_1(0) = 1$, $\Gamma = 0.03$, J=1. Black line: g=1.5, orange line: g=3 .

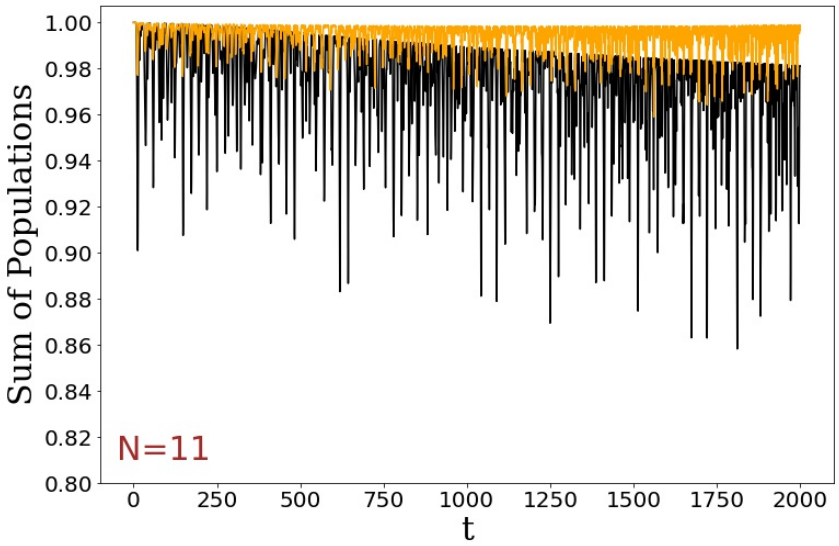

FIGURE 4.9: Sum of populations of a 11-qubit chain connected to a Square of Lorentzian reservoir for $c_1(0) = 1$,$\Gamma = 0.03$, J=1. Black line: g=1.5, orange line: g=3 .

In Fig 4.6-4.7, we study the population dynamics in the $g > J$ regime. It is easily observed that, the oscillations of the first and the channel qubit are almost complementary. In this case, the population is essentially trapped inside the first 4 qubits with a negligible amount leaking to the last qubit as shown in the blue line. These findings suggest that the evolution of the last qubit freezes at high coupling strengths, alluding to a phenomenon known as the quantum zeno effect, which effectively prevents the reservoir's total decay through the final qubit. It must be

noted that this freezing of the population was also observed by Mouloudakis and Lambropoulos when studying qubit chains interacting with two Lorentzian reservoirs through the first and last qubits. More specifically, the conditions needed for the freezing of the population inside the chain to happen were an initial excitation in any but the edge spins and coupling strengths that satisfy $g > J$. However, when the initial excitation was in either of the two edge spins, the population decayed very fast to the environment. When the coupling strengths g of the reservoirs are greater than the interaction J, the egde qubits behave like they are "cut-off" the chain and stop communicating with the intermediate qubits. It is almost like, the reservoir "steals" the qubit that it interacts with from the chain. Since the square of the Lorentzian is a more "exaggerated" version of the Lorentzian, one would expect similar behaviors of the two reservoirs, and this is exactly what happens, with the only difference being that our model has only one reservoir connected to the last qubit. If the initial excitation is in any of the first 4 qubits and $g > J$ is satisfied, then the last qubit can not communicate with the rest of the chain and the population stays trapped there.

In Fig 4.8, we study the total population of a 5 qubit chain for different values of g. As we can see, the freezing effect that was previously explained is intensified for higher values of g. Lastly, when increasing the length of the chain as depicted in Fig 4.9, the decay does not seem to slow down as we would expect, however the oscillations of the total population are now of smaller amplitude.

4.2 Revisiting the Lorentzian squared QSD

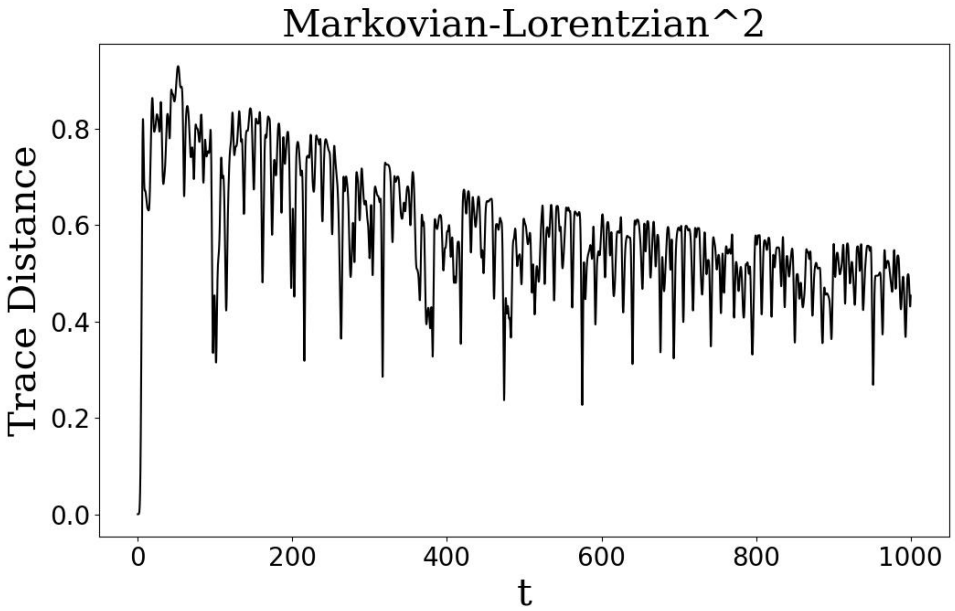

FIGURE 4.10: Trace Distance between Markovian and Lorentzian squared for a 5-qubit chain and qubit-qubit coupling J=1. The parameters used in each case are: Markovian reservoir with $\Gamma_M = 0.01$, Lorentzian squared reservoir with g=1, $\Gamma = 0.03$ and $\Delta_c = 0$.

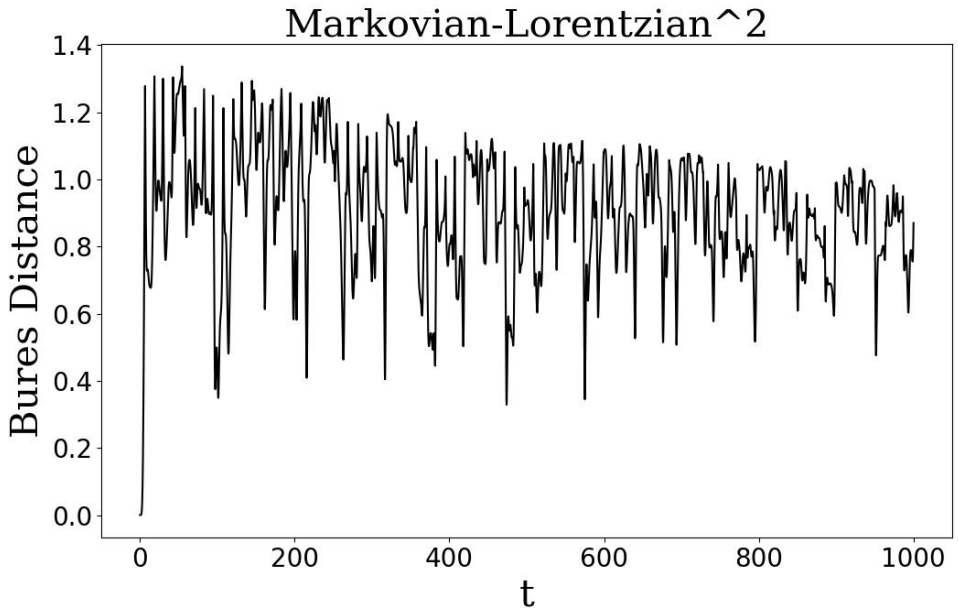

FIGURE 4.11: Bures Distance between Markovian and Lorentzian squared for a 5-qubit chain and qubit-qubit coupling J=1. The parameters used in each case are: Markovian reservoir with $\Gamma_M = 0.01$, Lorentzian squared reservoir with g=1, $\Gamma = 0.03$ and $\Delta_c = 0$.

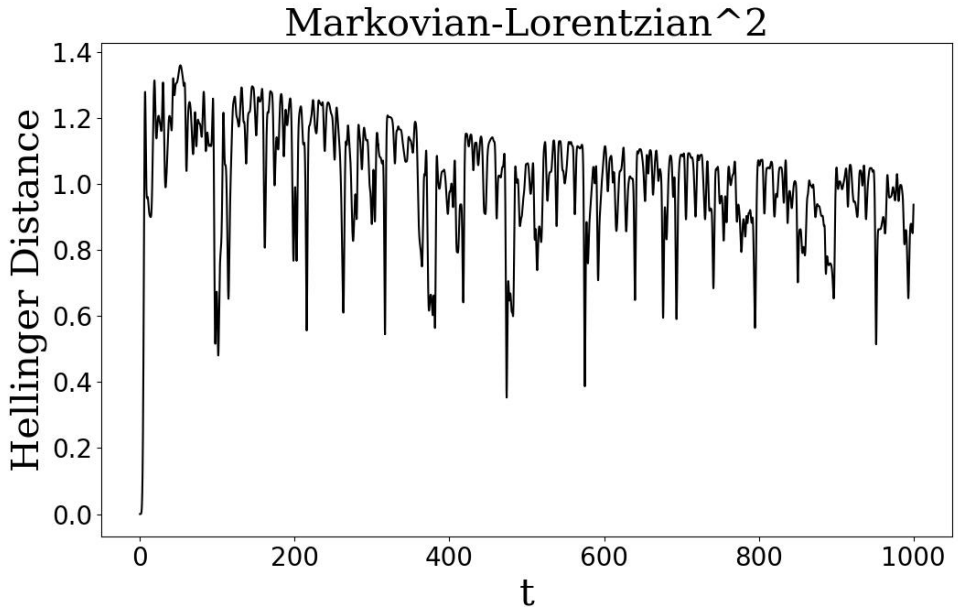

FIGURE 4.12: Hellinger Distance between Markovian and Lorentzian squared for a 5-qubit chain and qubit-qubit coupling J=1. The parameters used in each case are: Markovian reservoir with $\Gamma_M = 0.01$, Lorentzian squared reservoir with g=1, $\Gamma = 0.03$ and $\Delta_c = 0$.

Now, we return again to the Trace distance for a 5-qubit chain with a Lorentzian squared reservoir connected to the last qubit, but this time with $\Gamma = 0.03$. Figure 4.10 unveils intriguing insights into the non-Markovian dynamics induced by the

Lorentzian squared reservoir. The decay observed in this distance metric is significantly slower compared to previous cases, indicating a much more prolonged interaction between the quantum system and its environment. This markedly slower decay underscores an exceptionally high degree of non-Markovianity, suggesting that the system retains memory of its past states for an extended period.

Fig 4.11-4.12 depict the Bures and Hellinger metrics, respectively, offering complementary perspectives on the non-Markovian dynamics induced by the Lorentzian squared reservoir. These metrics exhibit similar oscillatory behavior to the Trace Distance, albeit with slightly slower decay rates as we showed in previous chapters.

One remarkable feature of the Lorentzian squared reservoir is its propensity to sustain non-Markovian behavior over extended time periods. This sustained interaction fosters the emergence of steady states within the quantum system, wherein quantum coherence and entanglement are preserved over time. The establishment of steady states suggests the existence of robust reservoir-induced coherence, which can have profound implications for quantum information processing tasks.The Lorentzian squared reservoir emerges as a potent source of non-Markovian dynamics, capable of sustaining steady states and preserving quantum coherence over extended time scales.

Chapter 5

Summary

In this thesis we studied the degree of non-Markovianity of reservoirs with various density of states. In order to provide a study pertainig to realistic systems, we explored the effect of the reservoirs on systems of interacting qubit chains connected to reservoirs in suitably chosen arrangements. Our analysis included quantum state measures as well as the time evolution of entanglement. In addition to typical reservoirs, such as Markovian, Lorentzian and Ohmic, we also conducted a detailed investigation of the Lorentzian squared reservoir, a rather unusual reservoir which was found to exhibit surprising properties.

Using an XX chain of interacting qubits coupled to reservoirs as a practical model for quantum information processing, the study employed the density matrix formalism through the solutions to the Schrödinger equation to compute QSD measures. The evaluation of DNM involved comparing system evolution under non-Markovian and Markovian reservoirs. This comparison necessitated a judicious selection of the parameters of the spectral densities of the reservoirs involved in each QSD calculation. Beginning with a single-qubit coupled to a reservoir, we proceeded to the exploration of the interplay between the qubit-qubit coupling and qubit-reservoir interaction. Our analysis revealed slightly higher DNM values for all three reservoirs when measured using the Hellinger and Bures metrics compared to the trace distance measure. Our results revealed differences in DNM between single-qubit and five-qubit chain analyses, with larger systems exhibiting higher DNM due to excitation retention among interacting qubits.

Interestingly, the Ohmic reservoir exhibited significantly lower DNM across all three measures, suggesting a Markovian-like behavior due to the absence of noticeable back-flow of excitation from the reservoir to the qubit.

The Lorentzian and Lorentzian squared reservoirs, based on all three measures, displayed a similar DNM. This might appear contrary to expectations, given that the squared Lorentzian profile is more sharply peaked than the Lorentzian with the same parameters, implying a higher DNM. However, in our comparative analyses in Fig (3.9-3.14), the Lorentzian squared used was not the direct square of the accompanying Lorentzian, as adjustments in parameters were made as explained at the beginning of the chapter. When we calculated the evolution of the qubit excitation dynamics and DNM for the Lorentzian squared using the same Γ as the Lorentzian the we found a significantly higher DNM for the Lorentzian squared. Moreover, introducing $\Gamma = 0.03$ in the Lorentzian squared reservoir analysis shed light on sustained entanglement dynamics over extended time periods, uncovering intriguing insights into entanglement preservation.If it were possible to engineer a squared Lorentzian reservoir coupled to an open system, dissipation would diminish significantly. Our exploration of the Lorentzian squared spectral density goes beyond a theoretical exercise. It stems from the detection of non-Lorentzian line

shapes (Whipple, 1981, Pellegrino and al., 2020), such as the Lorentzian squared, although in different physical context.

Bibliography

Abdi, M. and M. B. Plenio (2018). In: *Phys. Rev. A* 98, 040303(R).
Dajka, J., J. Łuczka, and P. Hänggi (2011). In: *Phys. Rev. A* 84, p. 032120.
Goldberger, M. L. and K. M. Watson (1964). *Collision Theory*. New York: Wiley.
Jozsa, R. (1994). In: *J. Mod. Opt.* 41, p. 2315.
Lambropoulos, P. and D. Petrosyan (2007). *Fundamentals of Quantum Optics and Quantum Information*. Springer Verlag.
Leggett, A. J. et al. (1987). In: *Rev. Mod. Phys.* 59, p. 1.
— (1995). In: *Rev. Mod. Phys.* 67, p. 725.
Mendonça, P. E. M. F. et al. (2008). In: *Phys. Rev. A* 78, p. 052330.
Mouloudakis, G., T. Ilias, and P. Lambropoulos (2022). In: *Phys. Rev. A* 105, p. 012429.
Mouloudakis, G. and P. Lambropoulos (2021). In: *Quantum Inf. Process.* 20, p. 331.
— (2023). In: *Physical Review A* 106.5, p. 053709.
Mouloudakis, G., I. Stergou, and P. Lambropoulos (2023). In: *Physica Scripta* 98.8, p. 085111.
Nielsen, M. A. and I. L. Chuang (2000). *Quantum Computation and Quantum Information*. Cambridge: Cambridge University Press.
Paganelli, S. et al. (2013). In: *Phys. Rev. A* 87, p. 062309.
Pellegrino, D. and et al. (2020). In: *Phys. Rev. Lett.* 124, p. 123902.
Rivas, Á., S. F. Huelga, and M. B. Plenio (2014). In: *Rep. Prog. Phys.* 77, p. 094001.
Uhlmann, A. (2000). In: *Phys. Rev. A* 62, p. 032307.
Weiss, U. (2001). *Quantum Dissipative Systems*. Singapore: World Scientific.
Whipple, E. R. (1981). In: *Nucl. Inst. Meth.* 180, pp. 241–814.
Zou, H.-M. et al. (2020). In: *Phys. Scr.* 95, p. 085105.